Supplementary Information

Temperature-Dependent Reversible Structural Dynamics in Covalent Organic Framework Revealed by Cryogenic Infrared Spectroscopy.

Silas O. Frimpong, [a] Nathan McLane,[b] Matthew Dietrich, [a] Garrison Bauer, [a] Michael Baptist [a], Leah G. Dodson* [a], and Mercedes K. Taylor * [a]

[a] Department of Chemistry and Biochemistry, University of Maryland, College Park, MD 20742, USA.
[b] Institute for Physical Science and Technology, University of Maryland, College Park, MD 20742, USA.

Corresponding author*

Table of Contents

General Methods:

Anhydrous tetrahydrofuran (THF) and anhydrous *N*,*N*-dimethylformamide (DMF) were purified in an Inert Pure Solv solvent purification system before use. All other chemicals and solvents were purchased from Sigma-Aldrich, ThermoFisher and TCI and were used without further purification.

NMR Techniques:

Solution-state ^{1}H and ^{13}C NMR spectra were collected on a Bruker 400 MHz instrument. Chemical shifts are reported in parts per million (ppm) and are referenced to the solvent peaks $CDCl_3$ or DMSO-d_6.

High-resolution solid-state nuclear magnetic resonance (NMR) spectra were collected on a Bruker Avance NEO 500 MHz spectrometer with a double resonance HX probe. Cross-polarization (CP) with magic-angle spinning (MAS) was used to acquire the ^{13}C spectra. Powder samples were packed in a 3.2 mm regular wall zirconia MAS rotor with an SP1 drive cap. The magic angle spinning rate was 14 kHz. Proton-carbon matched cross polarization ramp was at 50 kHz with 2 ms contact time. The proton dipolar decoupling was achieved by applying continuous wave small phase incremental alternation with 64 steps (SPINAL-64) on the ^{1}H channel during acquisition. The 90-degree pulse length was 2.5 μs for ^{1}H and the recycle delay was 5 s. The ^{13}C chemical shifts are given relative to tetramethylsilane as zero ppm using the methylene carbon of adamantane assigned to 38.2 and 28.7 ppm as reference. Each spectrum was collected with 2k scans.

X-ray Diffraction Measurements:

Powder X-ray diffraction patterns of COFs were collected on a Bruker D8 Advance diffractometer. The powder was mounted on a sample holder and exposed to X-rays using Cu Kα source (λ = 1.5406 Å, 40 kV and 40 mA). The PXRD patterns for the 3D COFs were recorded from 5° to 50° (2θ) with a step of 0.02° under ambient conditions in air.

Gas Sorption Measurements:

Gas adsorption isotherms were measured on a Micromeritics ASAP 2020 Plus adsorption analyzer. An oven-dried analysis tube with a glass filler rod was evacuated to a constant pressure of 9 μbar on the adsorption analyzer after which the mass of the evacuated tube and rod was obtained.

Approximately 120 mg of the sample was measured out in air and transferred to the analysis tube, which was then activated at 120 °C at inert atmosphere overnight on a Schlenk line. The sample with the rod was further activated on the adsorption analyzer at 120 °C under vacuum overnight. After activation, the tube's mass was measured again to obtain the exact mass of the activated sample. The analysis tube with the rod and sample was then attached to the analysis port of the instrument for the surface area measurement. A liquid nitrogen bath (77 K) was used for the isotherms. Brunauer-Emmett-Teller (BET) was used to determine the specific surface area (m^2/ g).

Scanning Electron Microscopy Imaging:

Scanning electron microscopy (SEM) images were collected using a Hitachi SU-70 FEG instrument. Dry powder samples were deposited onto carbon tape attached to a sample holder. Samples were then coated with gold/palladium for 10 minutes to ensure that the samples did not charge during image collection.

Sample Preparation for Cryogenic FTIR Analysis:

To allow for transmission Fourier-transform infrared (FTIR) spectroscopy of these porous materials, the pure sample materials were diluted in potassium bromide (KBr) powder (purchased from WardScience) and crushed into fine dust. The mixture was then loaded into a die, and a pressure of 12 tons/in^2 was applied from a Carver hydraulic press to create a 1-inch diameter, transparent, sample-KBr pellet of thicknesses ranging from 0.025-0.075 inches. Peaks assigned to known impurities in the KBr pellets (due to water and carbon dioxide) are marked with asterisks in the figures in the main text. Figure S16 shows these peaks as they appear in KBr pellets without added framework materials. The peaks become significantly more pronounced at lower temperatures. After pressing, the pellets were placed inside the FTIR sample chamber (and heated to 127 °C under vacuum for two hours, then cooled to room temperature while vacuum was maintained for two additional hours, to ensure complete evacuation of the pores.

Computational Methods:

Calculation of vibrational frequencies:

Cluster models for each covalent organic framework were created that represented the framework's repeating unit. Terminal bonds that would leave the unit cell are truncated with hydrogen atoms.

In the case of COF-300, the cluster model consists of a central quaternary carbon there are four 1,4-phenylenebis(*N*-phenylmethanimine) units (Scheme S1). For its reduced counterpart, COF-300-amine, the cluster model consists of four *N*-[4-(anilinomethyl)benzyl] aniline units stemming from a central carbon (Scheme S1). For COF-V, a central benzene ring connects three 1-(4-(iminomethyl)-2,5-divinylphenyl)-*N*-phenylmethanimine groups (Scheme S1). Images of the constructed cluster models are presented in Figure S17.

Figures S11–S13 show a comparison of the experimental spectra obtained for each material (COF-300, COF-300-amine, and COF-V, respectively) at two temperatures (room temperature, RT in red and 30 K in blue) with the simulated spectrum obtained from the cluster model designed to represent each framework (plotted in green). The simulated spectrum was obtained by convolving the vibrational stick spectrum with a Gaussian lineshape (FWHM = 11.7 cm^{-1}) for comparison with experiment. The comparison of the experimental spectra with the simulated spectrum enabled identification of the normal modes that are most affected by changes in temperature. Cartesian coordinates of the optimized cluster models, along with the corresponding calculated frequencies, are available in the extended data repository (FigShare DOI: 10.6084/m9.figshare.26510275.v1).

Structural changes in the materials can lead to complicated changes in vibrational frequencies that are not necessarily intuitive but can be revealed through quantum-chemistry calculations. The effect of the pedal motion on the materials' vibrational frequencies was simulated through the dihedral-angle-dependent calculations, as discussed in the main text. The full simulated spectra at each of the three angles (0°, red; 10°, yellow; 20°, blue) are shown for each molecular fragment (Figures S14 and S15 for *N*-benzylideneaniline and *N*-benzylaniline, respectively). The vibrational frequencies from each fragment at each angle are tabulated in Tables S1 and S2. Additionally, the change in vibrational frequency for dihedral angle X=10° or 20° with respect to 0° ($\Delta(X°-0°)$) are reported. Cartesian coordinates of the molecular fragments at different dihedral angles, and associated frequencies, are available in the extended data repository (FigShare DOI: 10.6084/m9.figshare.26510275.v1).

Modeling of structural representations of COFs:

The structures showing the dimensions and atomic arrangements of COF-300, COF-300-amine, and COF-V were built by BIOVIA Material Studio chemical structure modeling software (Figure 1). The molecular fragments too were modeled with this software (Figure S18). Using the universal

force field, these structures were geometrically optimized with the Forcite smart algorithm. The van der Waals and electrostatic interaction were atom-based. The optimization quality was set as ultra-fine.

Scheme S1. Components of cluster models for COF-300 (left), COF-300-amine (center), and COF-V (right).

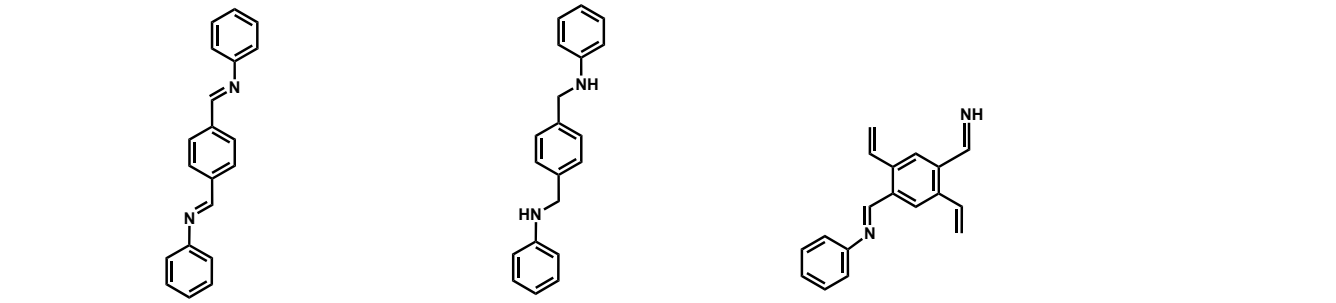

Monomer Synthesis:

Synthesis of tetraphenylmethane:

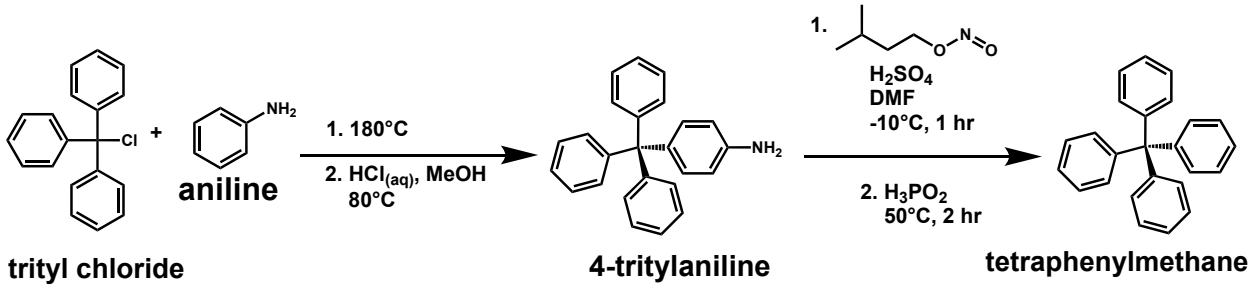

The synthesis of tetraphenylmethane was adapted from a known procedure. [1–3] Trityl chloride (10 g, 35.9 mmol) and aniline (9.4 mL, 104.1 mmol) were added to a 500 mL round bottom flask (RBF) equipped with a stir bar. The mixture was refluxed at 180 °C with a vigorous stirring until a violet solid formed. The heating was continued for an additional 10 minutes, after which the reaction was cooled to room temperature (r.t.). The solids were crushed into smaller pieces and then suspended in a 1:1 mixture of methanol and 2 M aqueous HCl (50 mL each). The violet suspension was further refluxed at 80 °C for 30 min. It was then cooled to r.t. and vacuum filtered, followed by washing with water, to obtain 4-tritylaniline as a light purple residue. The obtained solid was dried under vacuum at 70 °C overnight. In a 250 mL RBF, dried 4-tritylaniline was suspended in 105.6 mL DMF and stirred. The mixture was cooled to -10 °C (acetone/ice bath). Concentrated H_2SO_4 (18 M in water, 11.4 mL, 204.5 mmol) was added slowly, followed by

isopentyl nitrite (8.6 mL, 64.6 mmol). After the mixture was stirred at -10 °C for an hour, phosphinic acid (50% v/v, 15.4 mL, 140.6 mmol) was added dropwise. A brown cloudy mixture formed, which was warmed to r.t and further refluxed at 50 °C under stirring for 2 h. After bringing the reaction to room temperature, it was vacuum filtered and washed with DMF (2x), water, and ethanol. The product was dried under vacuum to yield tetraphenylmethane as a brown solid. Yield: (9.9 g, 86%). ^{1}H NMR (400 MHz, $CDCl_3$) δ = 7.27-7.18 (m, 20H).

Synthesis of tetrakis(4-nitrophenyl)methane:

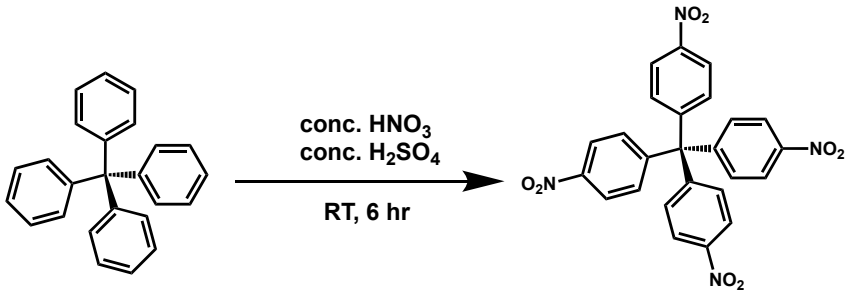

tetraphenylmethane **tetrakis(4-nitrophenyl)methane**

The synthesis of tetrakis(4-nitrophenyl)methane was adapted from a previous procedure. [1,4,5] Tetraphenylmethane (9.9 g, 30.9 mmol) was transferred to a 250 mL RBF in an ice bath equipped with a stir bar. In a separate 250 mL Erlenmeyer flask, also cooled to 0 °C, a mixture of 15.7 M HNO_3 (41.1 mL, 624.2 mmol) and 18 M H_2SO_4 (19.9 mL, 358.4) was made. The acid mixture was carefully added dropwise to the tetraphenylmethane at 0 °C. The reaction mixture was brought to r.t. and stirred for 6 h. It was then placed in an ice bath and diluted with ~35 mL of deionized water. Using a fine porous fritted funnel, the resulting mixture was vacuum filtered and washed with a large amount of water. The resulting solid was recrystallized in THF to yield (6.2 g, 40%) of tetrakis(4-nitrophenyl)methane. ^{1}H NMR (400 MHz, CDCl3) δ = 8.24-8.23 (d, 8H), 7.43-7.41 (d, 8H).

Synthesis of tetrakis(4-aminophenyl)methane (TAPM):

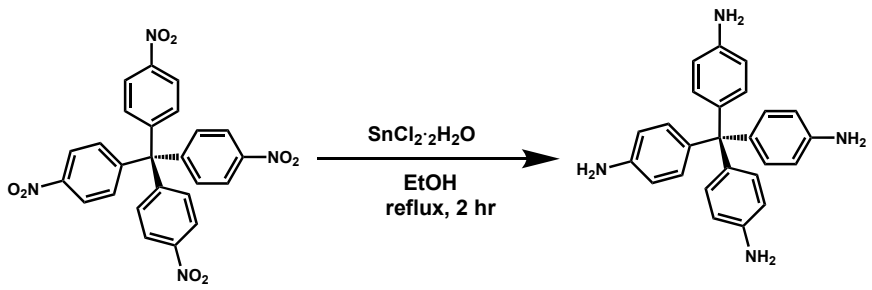

tetrakis(4-nitrophenyl)methane **Tetrakis(4-aminophenyl)methane(TAPM)**

The synthesis of tetrakis(4-aminophenyl)methane was adapted from a reported procedure.[5–7] Tetrakis(4-nitrophenyl)methane (6.2 g, 12.4 mmol) was dissolved in 618 mL of ethanol in a 1 L RBF. Tin chloride dihydrate (55.8 g, 247.2 mmol) was added to the reaction mixture, which was refluxed at 90 °C for 2 h. After bringing the reaction mixture to r.t., ethanol was removed under reduced pressure. The mixture was diluted with ~200 mL of water and cooled to 0 °C, followed by the addition of 10% aqueous sodium hydroxide (w/w) until pH was approximately 10. The mixture was brought to r.t. and allowed to stir overnight to hydrolyze all tin salts. The resultant mixture was vacuum filtered and washed with water, and the isolated solids were heated to 80 °C in ~300 mL of 1,4-dioxane to selectively dissolve tetrakis(4-aminophenyl)methane. The hot reaction mixture was vacuum-filtered to remove the solids, which were then washed with hot 1,4-dioxane to ensure that all traces of TAPM were collected in the filtrate. The 1,4-dioxane was then removed under reduced pressure. Water was added to the resultant mixture, forming a brownish product, which was vacuum-filtered. The solids were washed with a large amount of water, followed by ethanol wash to finally obtain tetrakis(4-aminophenyl)methane as a beige solid. Yield: (3.7g, 79.5%). 1H NMR (400 MHz, DMSO-d_6) δ = 6.67-6.66 (d, 8H), 6.39-6.37 (d, 8H), 4.85 (s, 8H).

Synthesis of 2,5-divinylterephthalaldehyde (DVA):

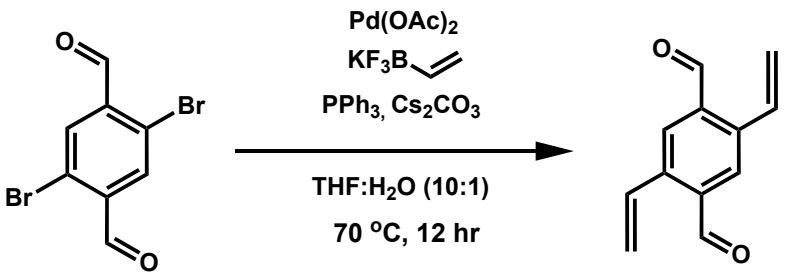

2,5-dibromoterephthalaldehyde **2,5-divinylterephthalaldehyde**

2,5-dibromoterephthalaldehyde (6.0 g, 20.6 mmol), potassium vinyltrifluoroborate (7.16 g, 53.445 mmol), cesium carbonate (33.35 g, 102.75 mmol), triphenylphosphine (0.826 g, 3.288 mmol), and pallidum acetate (0.369 g, 1.644 mmol) were dissolved in tetrahydrofuran (150 mL) and deionized water (15 mL). The resulting solution was heated to 70 °C under an argon atmosphere for 12 h.[8] The reaction mixture was diluted with deionized water, extracted with ethyl acetate three times, washed with brine, and dried with anhydrous magnesium sulfate. The crude product was purified via flash column chromatography with hexanes: ethyl acetate (5:1) to yield 2,5-divinylterephthalaldehyde (1.3 g, 51.82%) as a pale-yellow powder. ^{1}H NMR (400 MHz, d_6-DMSO) δ = 10.34 (s, 2H), 8.18 (s, 2H), 7.66-7.59 (m, 2H), 5.97 (d, 2H), 5.57 (d, 2H).

Synthesis of 1,3,5-tris-(4-nitrophenyl)benzene TNPB:

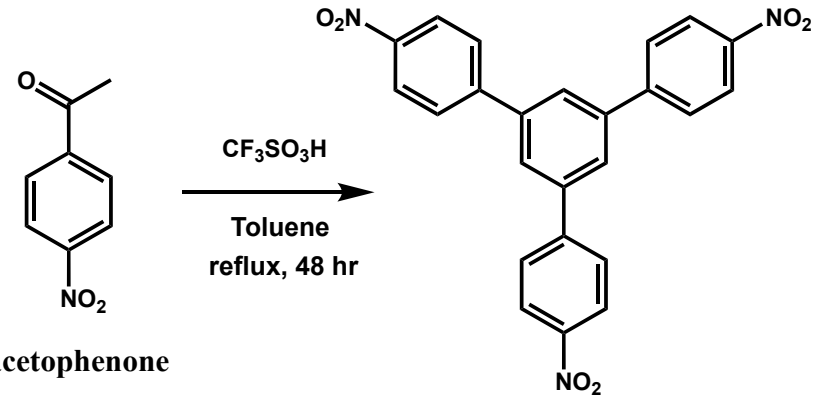

p-nitroacetophenone

1,3,5-tris-(4-nitrophenyl)benzene

Trifluoromethanesulfonic acid (4.0 mL, 45.6 mmol), *p*-nitroacetophenone (40 g, 242.4 mmol), and toluene (162 mL) were added to a flask with a Dean-Stark apparatus and reflux condenser attached. The resulting solution was refluxed for 48 h. [9] After allowing the reaction flask to cool, the solution

was filtered and washed with acetone to yield a black solid. The black solid underwent Soxhlet extraction with DMF for 72 h, to yield a yellow solid. ^{1}H-NMR was not obtained for the product as it is insoluble in common solvents.

Synthesis of 1,3,5-tris-(4-aminophenyl)benzene (TAPB):

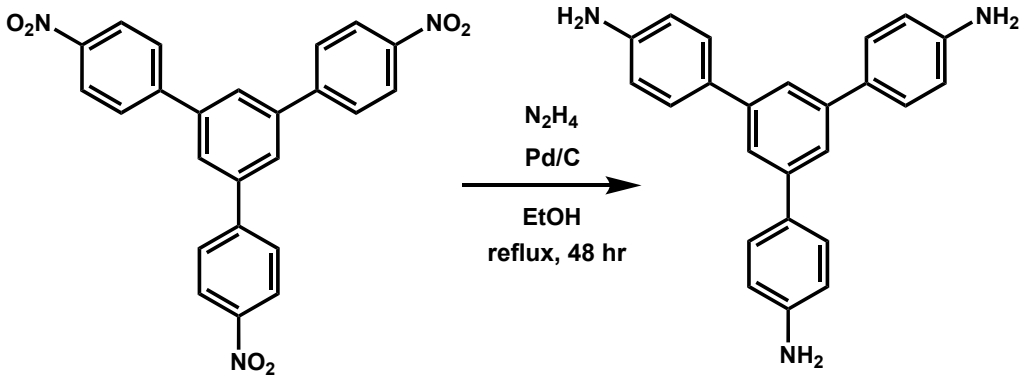

1,3,5-tris-(4-nitrophenyl)benzene **1,3,5-tris-(4-aminophenyl)benzene**

1,3,5-tris-(4-nitrophenyl)benzene (15.4 g, 34.9 mmol) and 10% Pd/C (1.5 g,14.0 mmol) were suspended in ethanol (420 mL) and heated to reflux. Hydrazine monohydrate (147.6 mL, 3038 mmol) was then added, and the reaction refluxed for 48 h. [9] The resulting solution was filtered through Celite, and the filtrate was concentrated by reduced pressure. The resultant slurry was filtered to yield 1,3,5-tris-(4-aminophenyl)benzene (10.6 g, 86%) as a white powder. ^{1}H NMR (400 MHz, d_6-DMSO) δ = 7.47 (t, 9H), 6.65 (d, 6H), 5.21 (s, 6H).

Synthesis of Covalent Organic Frameworks:

Synthesis of COF-300:

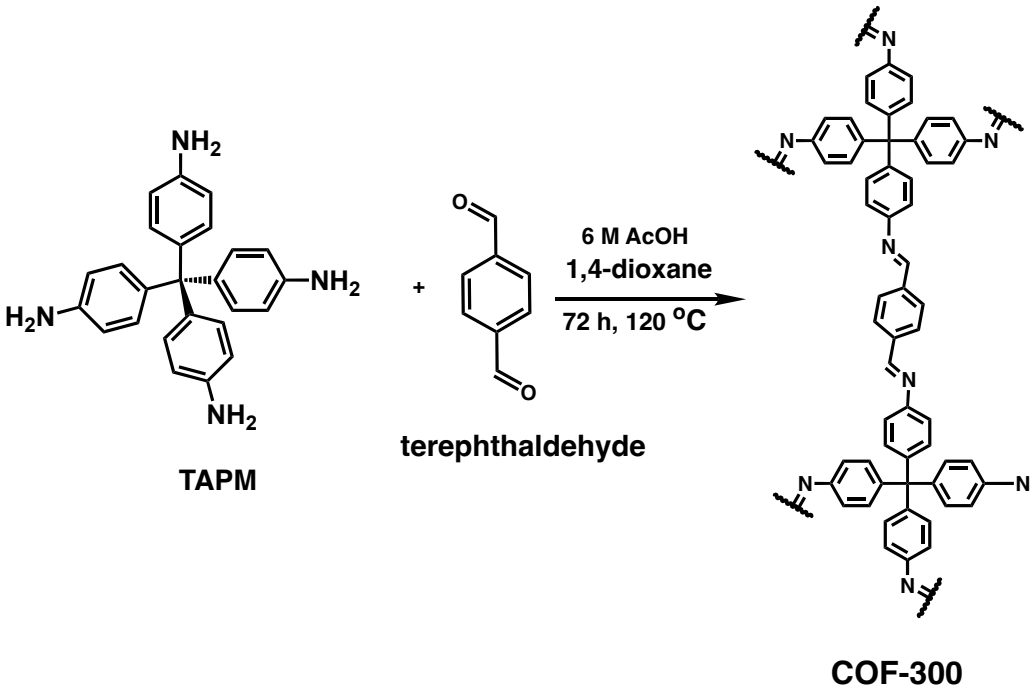

The synthesis of COF-300 was adapted from a literature procedure. [10] A 100 mL tubular solvent storage flask with a high vacuum valve was charged with tetrakis(4-aminophenyl)methane (0.50 mg, 1.32 mmol), terephthaldehyde (0. 35 g, 2.63 mmol), 6 M aqueous acetic acid (1.32 mL, 7.88 mmol), and 1,4-dioxane (13.30 mL). The flask was flash-frozen in liquid nitrogen at 77 K and evacuated to an internal pressure of 100 mTorr, then capped to create a closed system. The reaction mixture was heated at 120 °C for 72 h to obtain a yellow solid. The solid was vacuum-filtered and soaked in ~200 mL of 1,4-dioxane overnight. It was then vacuum filtered again and washed with acetone through Soxhlet extraction for 24 h affording a golden yellow COF-300 powder. Yield: 0.63 g. The product was characterized using powder X-ray diffraction (PXRD) (Figure S4), solid-state ^{13}C cross-polarization magic angle spinning (CP/MAS) NMR (Figure S1), scanning electron microscopy (SEM) (Figure S8), and Fourier transform infrared spectroscopy (FTIR) (Figure 2).

Synthesis of COF-300-amine:

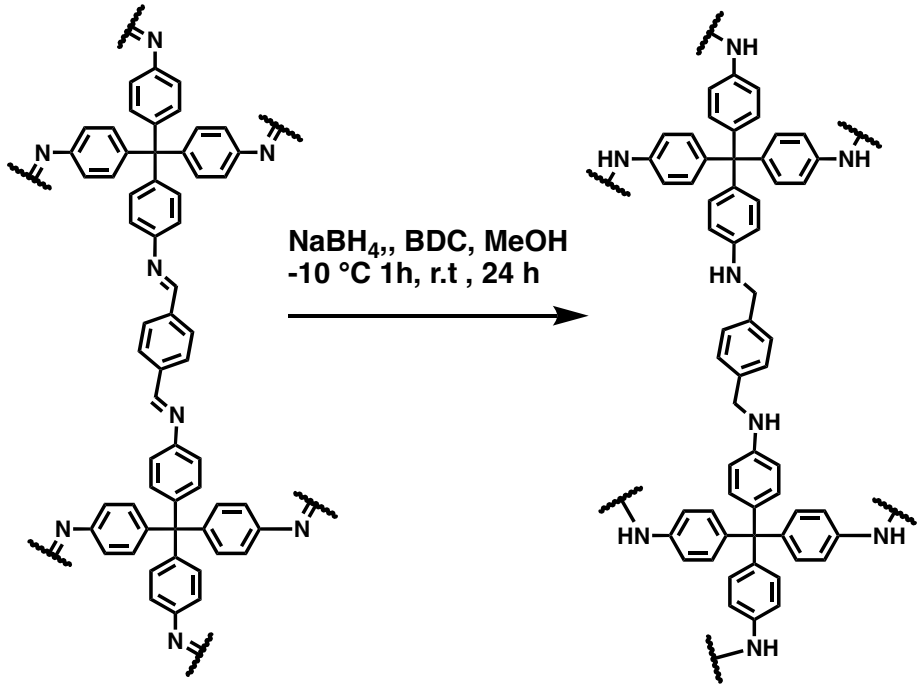

COF-300 **COF-300-amine**

The synthesis of COF-300-amine was adapted from a literature procedure. [7] COF-300 was activated under flowing argon at 120 °C overnight. Activated COF-300 (0.30 g, 2.08 mmol) was weighed in a glovebox and transferred to a Schlenk line, where it was put under argon. COF-300 was then suspended in 150 mL of anhydrous methanol. Terephthalic acid (0.35 g, 2.08 mmol) was added to the suspension and stirred at -10 °C for 5 min. Sodium borohydride (3.00 g, 79.12 mmol) was added in small portions over a 10 min period and stirred at -10 °C for 1 h. The reaction mixture was warmed to room temperature and allowed to stir for an additional 24 h. The solids were isolated through vacuum filtration and washed with a large amount of water (3x) to remove unreacted sodium borohydride. The solid residue was suspended in ethanol (75 mL) overnight and vacuum filtered with nylon filter paper (0.2 μm pore size) to obtain COF-300-amine as a light-yellow power. Yield: 0.3 g. The product was characterized using powder X-ray diffraction (Figure S5), solid-state ^{13}C cross-polarization magic angle spinning NMR (Figure S2), scanning electron microscopy (Figure S9), and Fourier transform infrared spectroscopy (Figure 5a).

Synthesis of COF-V:

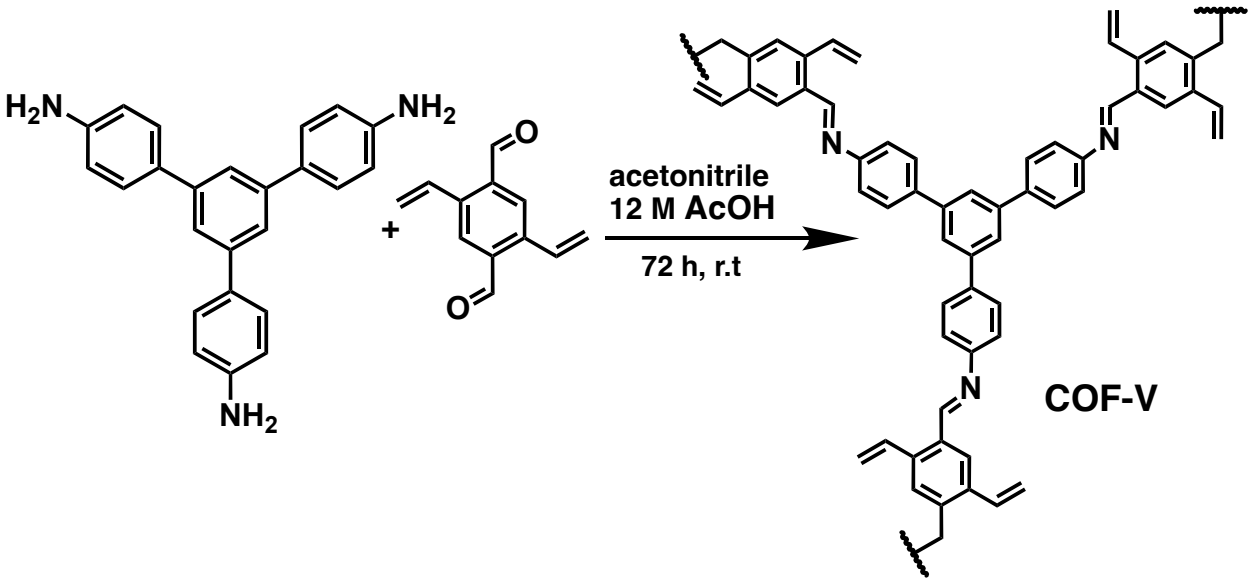

Synthesis of COF-V was Adapted from a literature procedure. [11,12] 2,5-divinylterephthalaldehyde (558.8 g, 3 mmol), 1,3,5-tris-(4-aminophenyl)benzene (702.8 g, 2 mmol) and acetonitrile (250 mL) were added to a 2 L media bottle and sonicated for 10 min. 12 M acetic acid (20 mL) was added to the solution and shaken vigorously for 2 mins. The solution was left undisturbed at r.t. for 72 h. The resulting yellow suspension was vacuum-filtered and washed via solvent exchange with tetrahydrofuran at 40 ^{o}C for 72h. The solvent was removed and replaced three times per day for three days, yielding COF-V as a bright yellow powder. Yield: 1.202 g. The product was characterized using powder X-ray diffraction (Figure S6), solid-state ^{13}C cross-polarization magic angle spinning NMR (Figure S3), scanning electron microscopy (Figure S10), and Fourier transform infrared spectroscopy (Figure 5b).

Supplementary Figures:

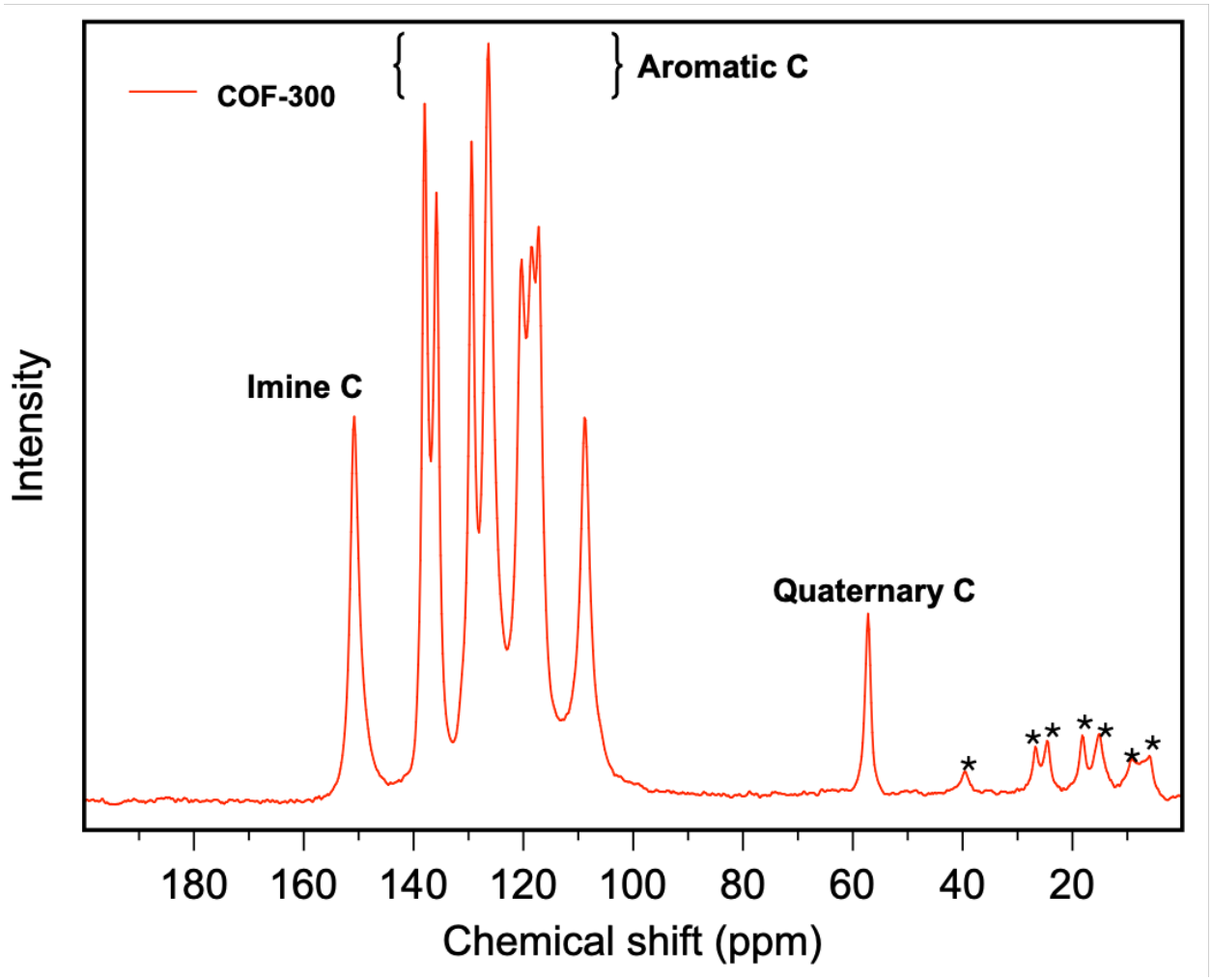

Figure S1. ^{13}C CP/MAS NMR spectrum of COF-300. Spinning sidebands are labeled with asterisks (*).

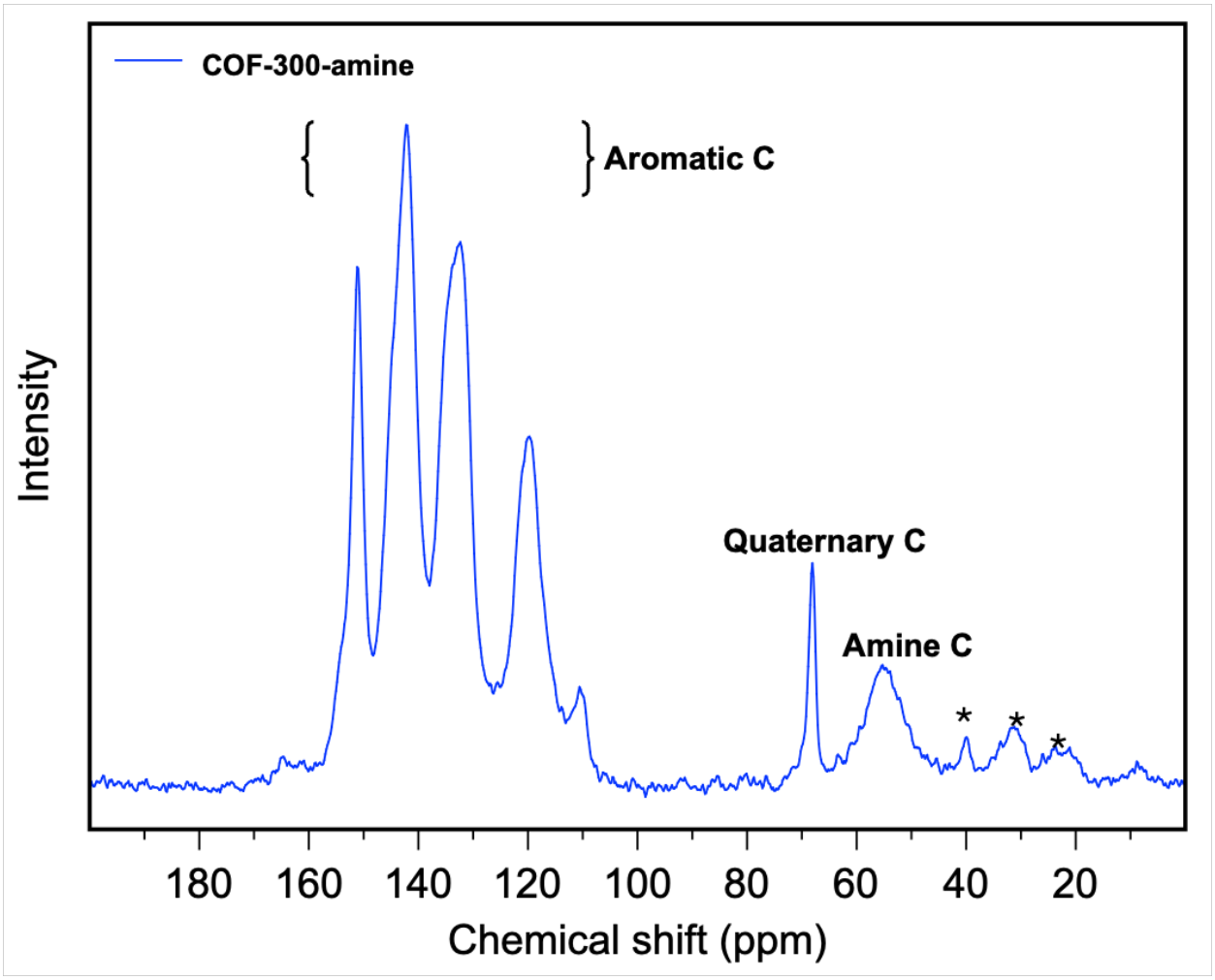

Figure S2. ^{13}C CP/MAS NMR spectrum of COF-300-amine. Spinning sidebands are labelled with asterisks (*).

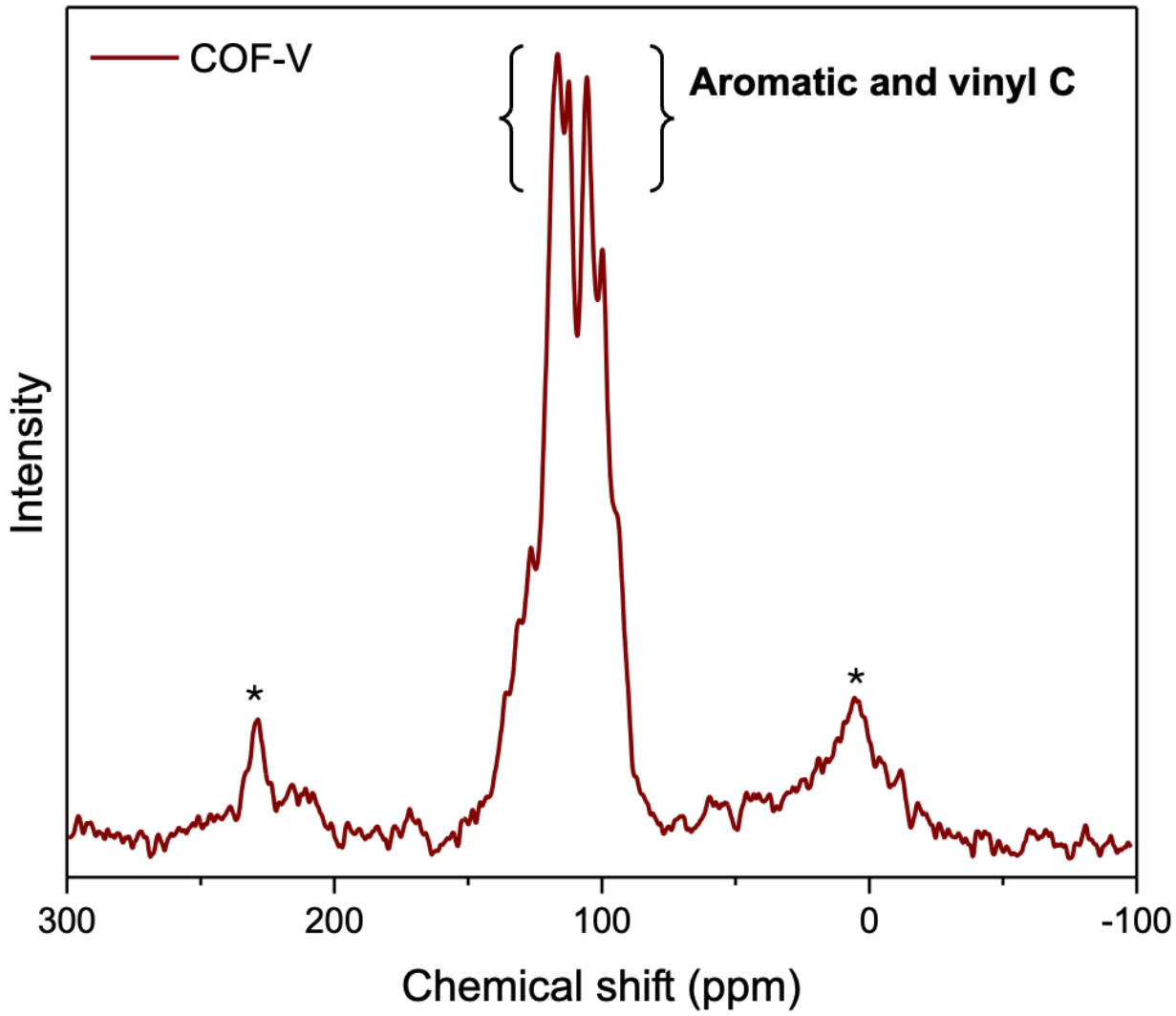

Figure S3. ^{13}C CP/MAS NMR spectrum of COF-V. Spinning sidebands are labelled with asterisks (*).

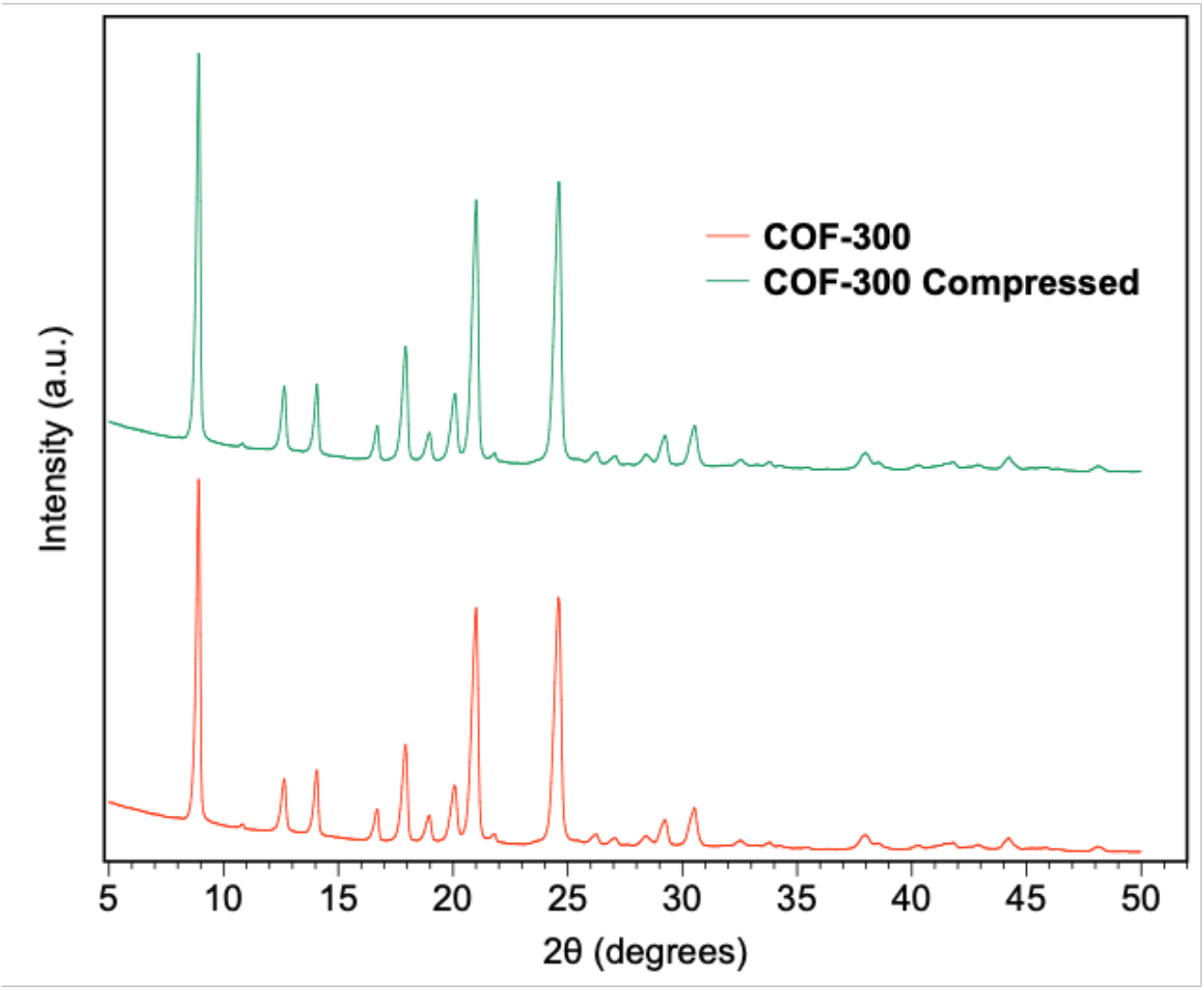

Figure S4. PXRD. Pattern of COF-300 and COF-300 compressed.

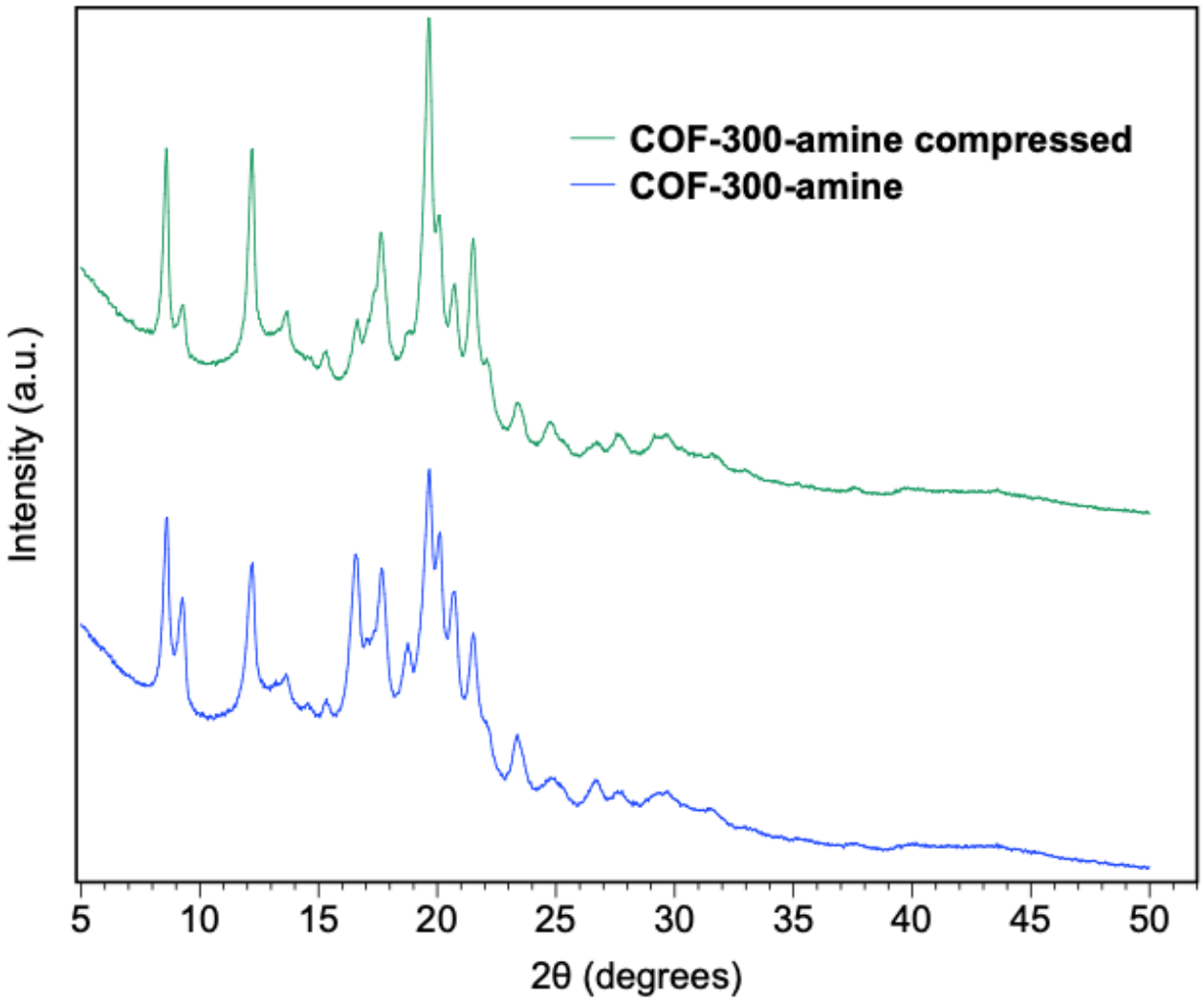

Figure S5. PXRD. Pattern of COF-300-amine and COF-300-amine compressed.

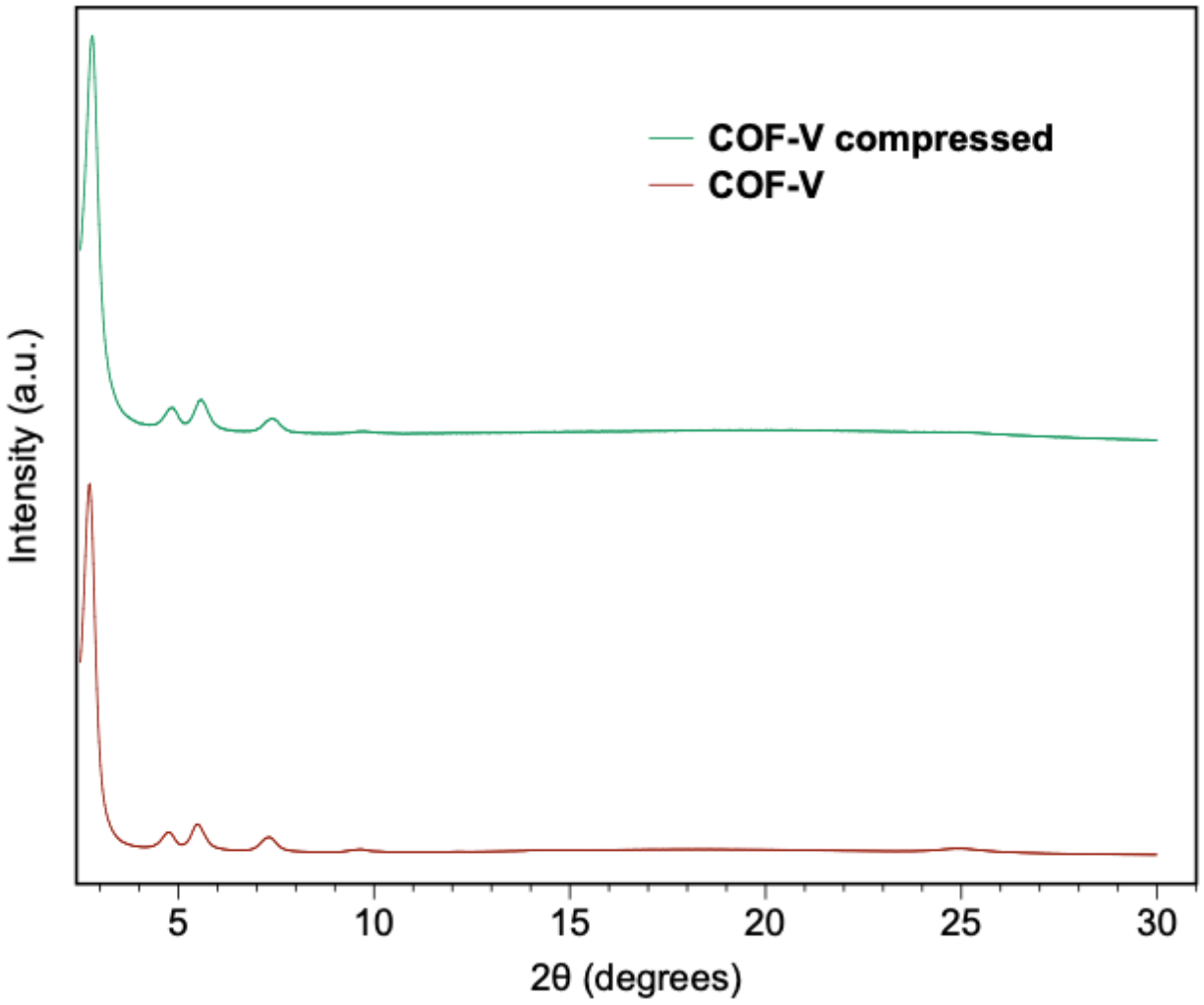

Figure S6. PXRD. Pattern of COF-V and COF-V compressed.

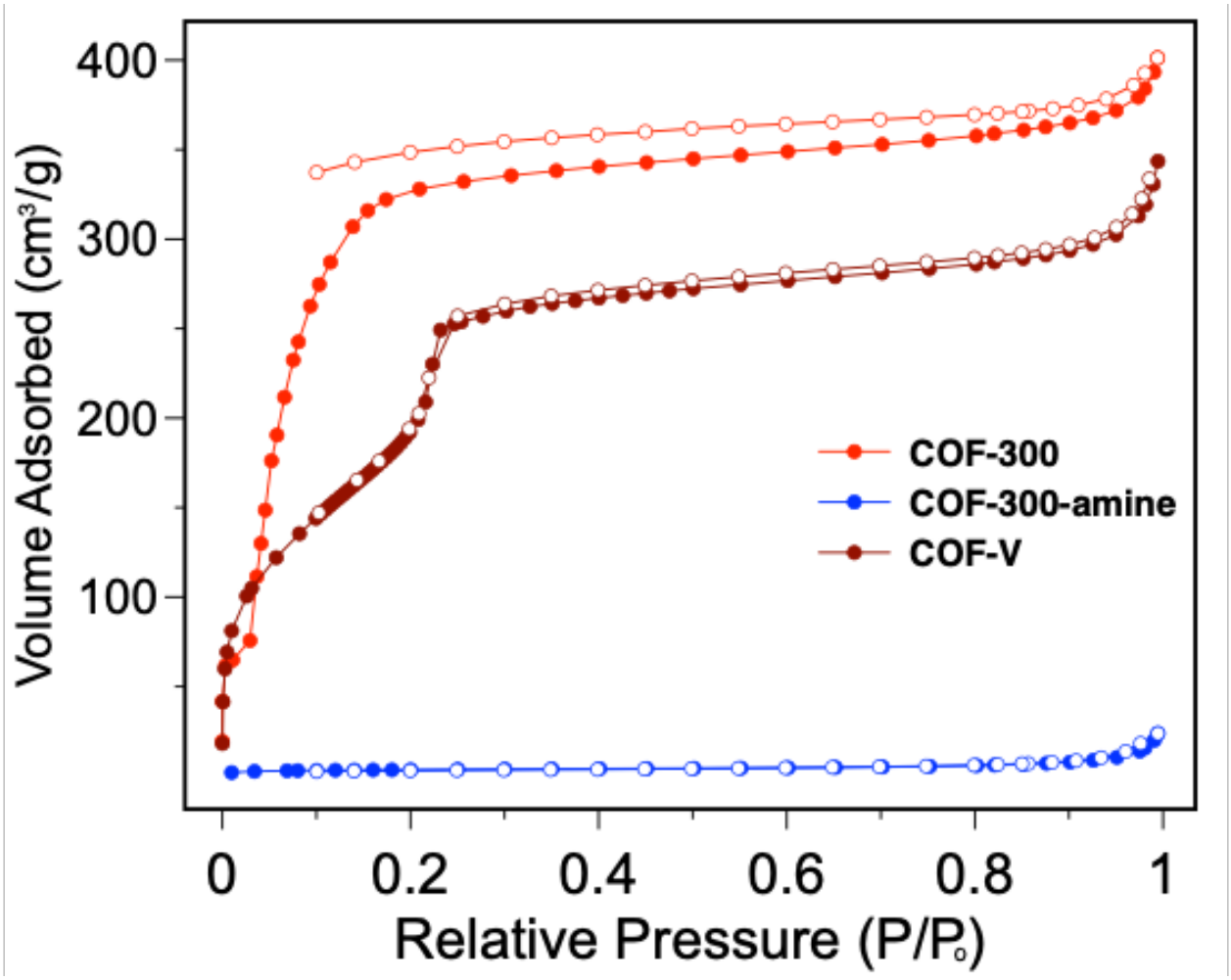

Figure S7. N_2 sorption measurement of COFs (red) COF-300, (brown) COF-300-V, (blue) COF-300-amine. Closed and opened circles represent adsorption and desorption respectively.

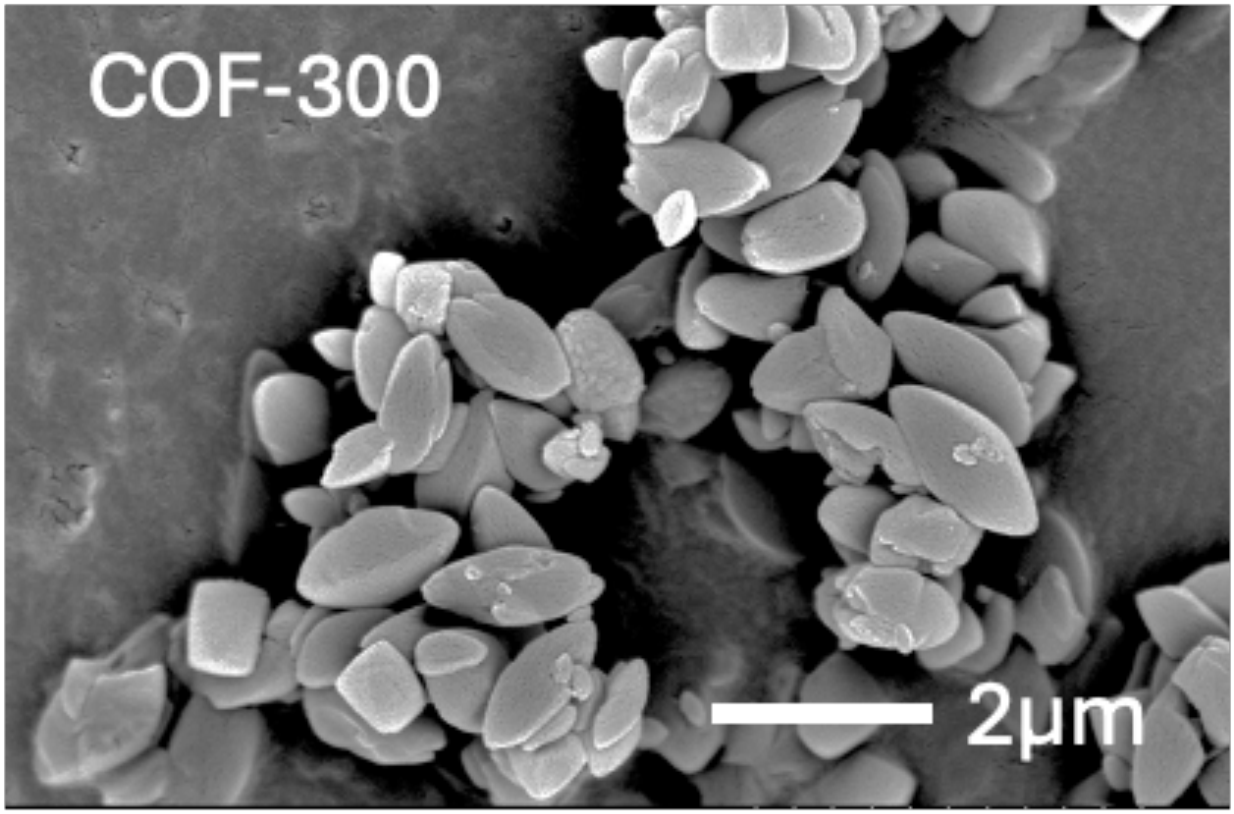

Figure S8. SEM image of COF-300.

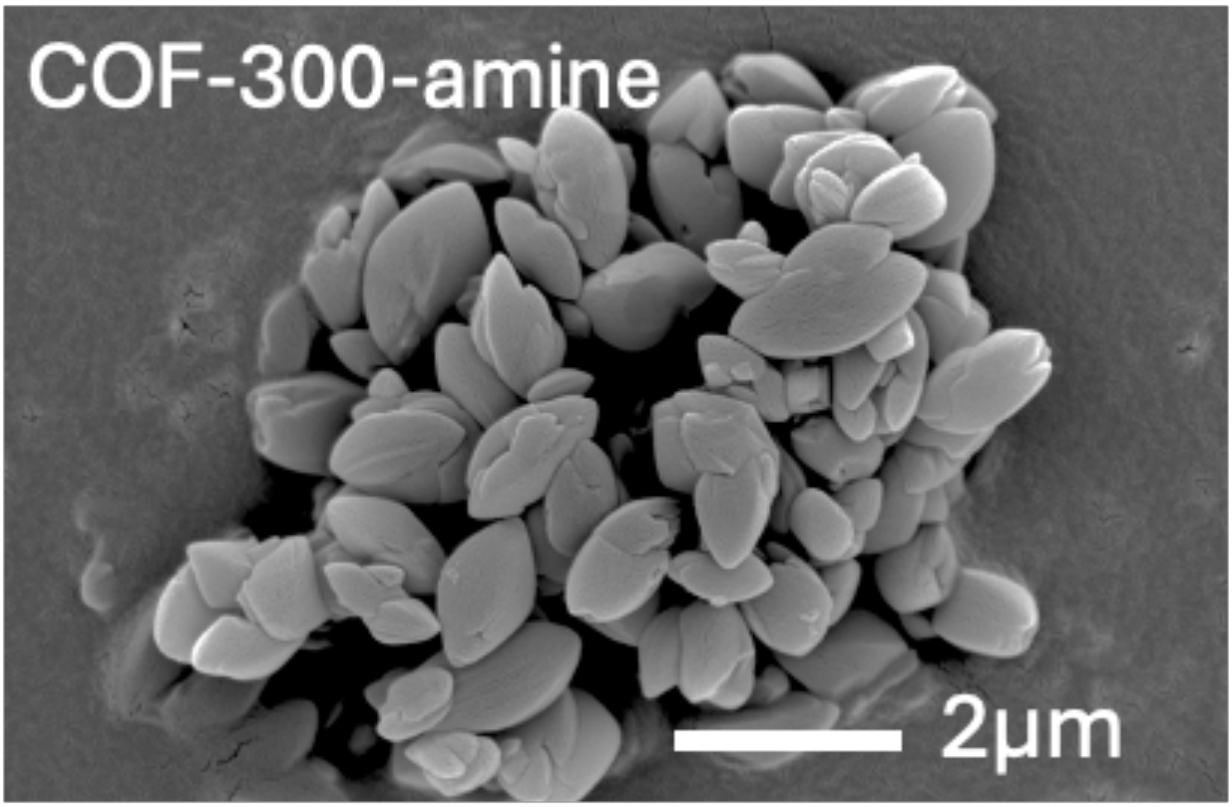

Figure S9. SEM image of COF-300-amine

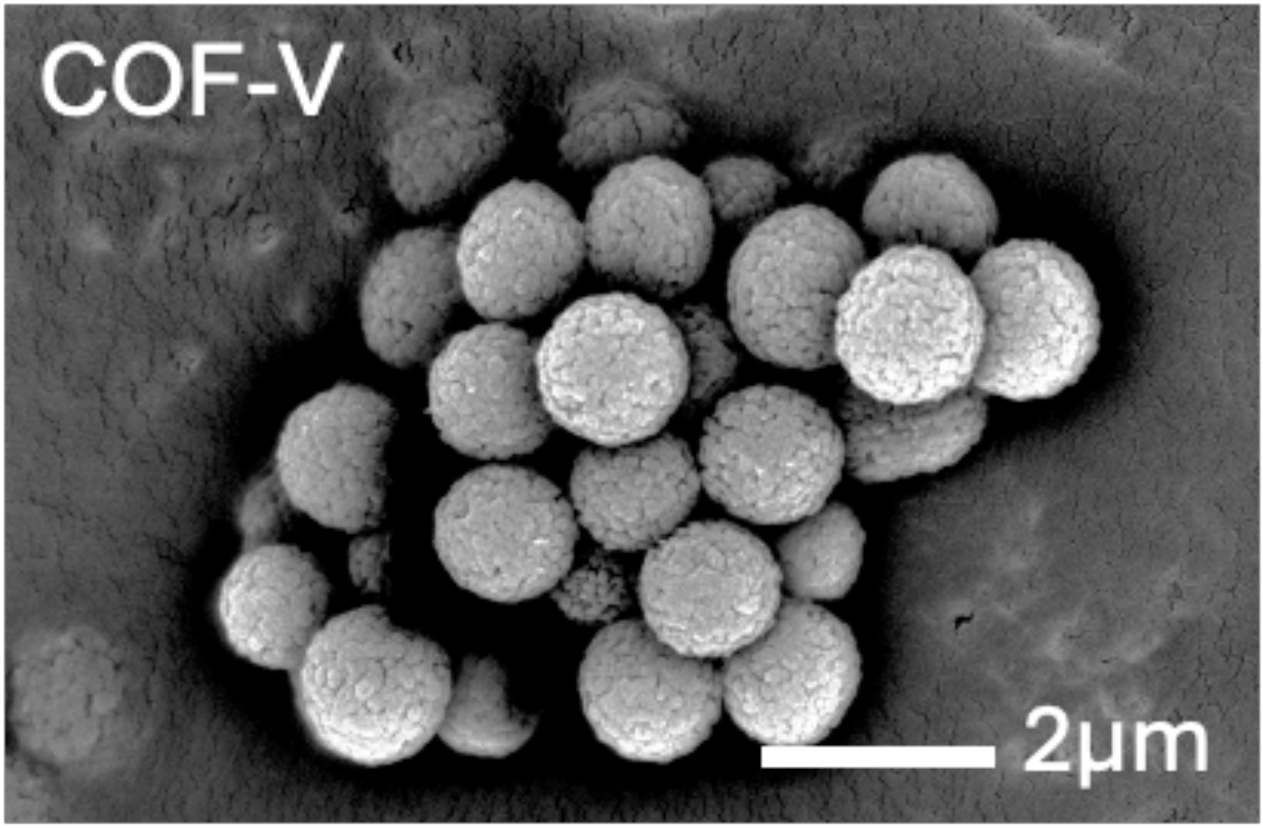

Figure S10. SEM image of COF-V

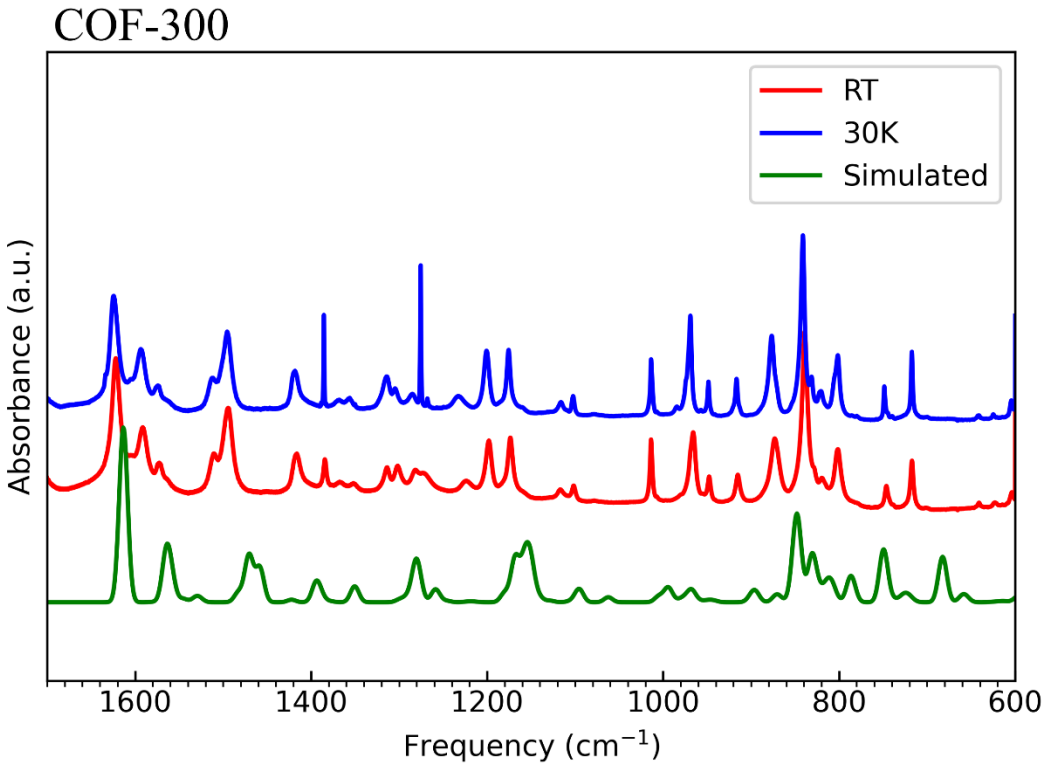

Figure S11. Comparison of the COF-300 experimental infrared spectra at two temperatures (RT = 298 K, red; 30 K, blue) with the simulated vibrational spectrum obtained from frequency calculations using the COF-300 cluster model. Calculations were carried out at B3LYP-DFT-D3/cc-pVTZ and stick spectra were convolved with a Gaussian lineshape for comparison with experiment.

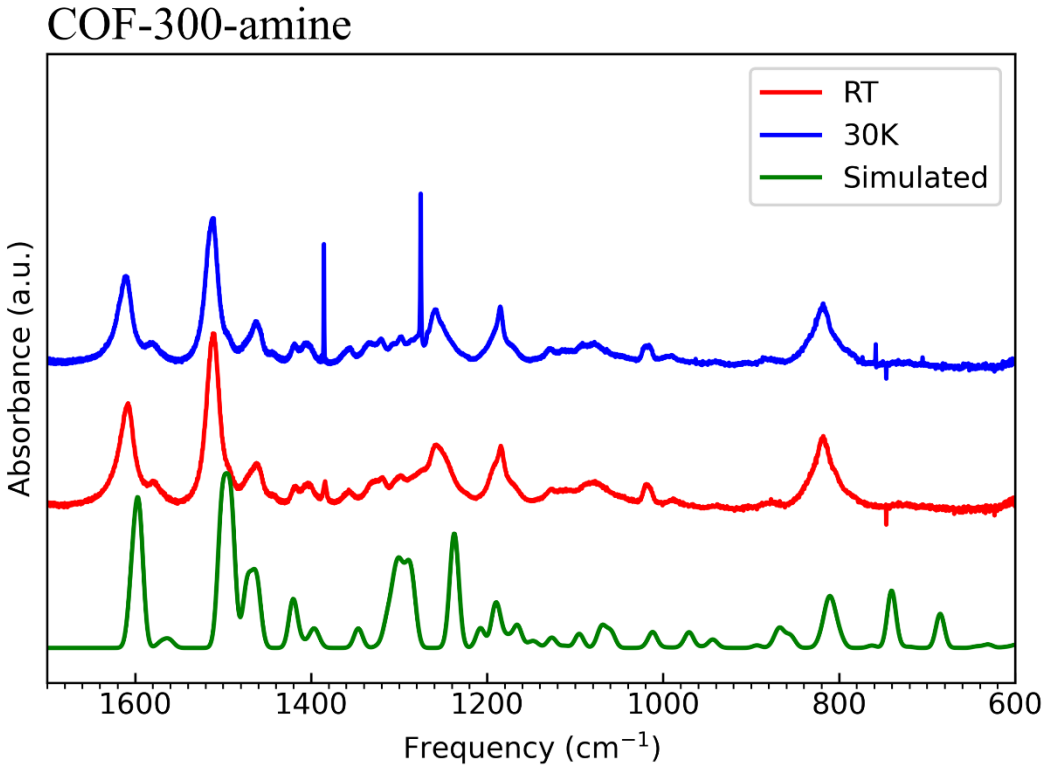

Figure S12. Comparison of the COF-300-amine experimental infrared spectra at two temperatures (RT = 298 K, red; 30 K, blue) with the simulated vibrational spectrum obtained from frequency calculations using the COF-300-amine cluster model. Calculations were carried out at B3LYP-DFT-D3/cc-pVTZ and stick spectra were convolved with a Gaussian lineshape for comparison with experiment.

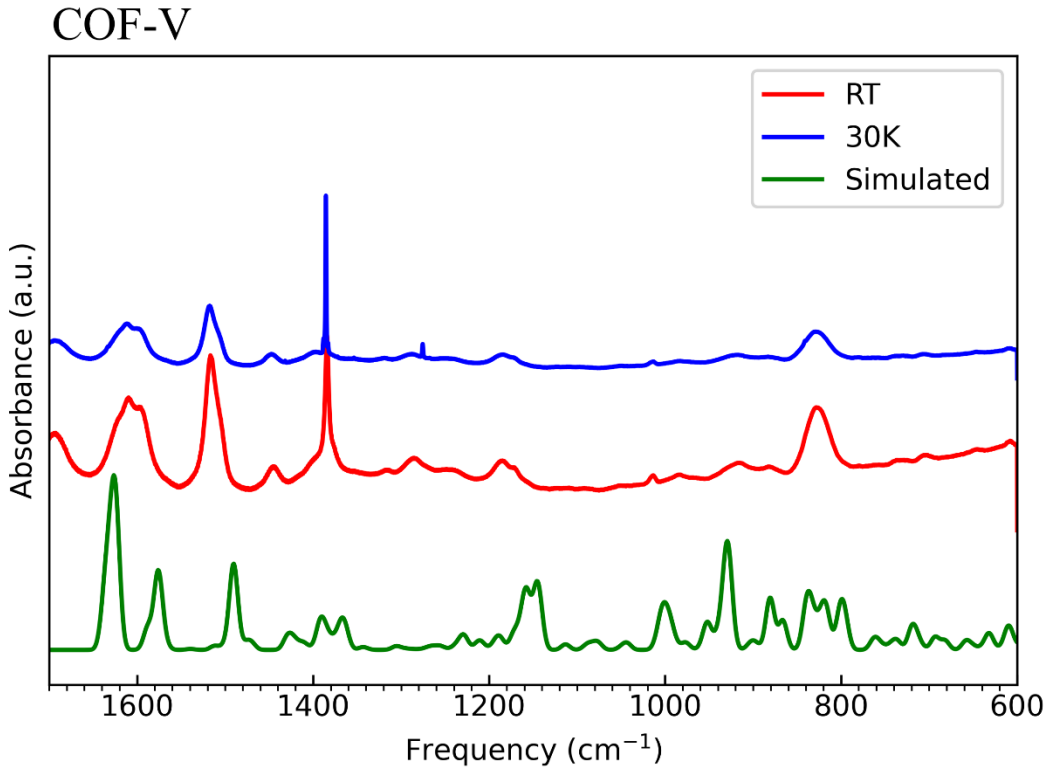

Figure S13. Comparison of the COF-V experimental infrared spectra at two temperatures (RT = 298 K, red; 30 K, blue) with the simulated vibrational spectrum obtained from frequency calculations using the COF-V cluster model. Calculations were carried out at B3LYP-DFT-D3/cc-pVTZ and stick spectra were convolved with a Gaussian lineshape for comparison with experiment.

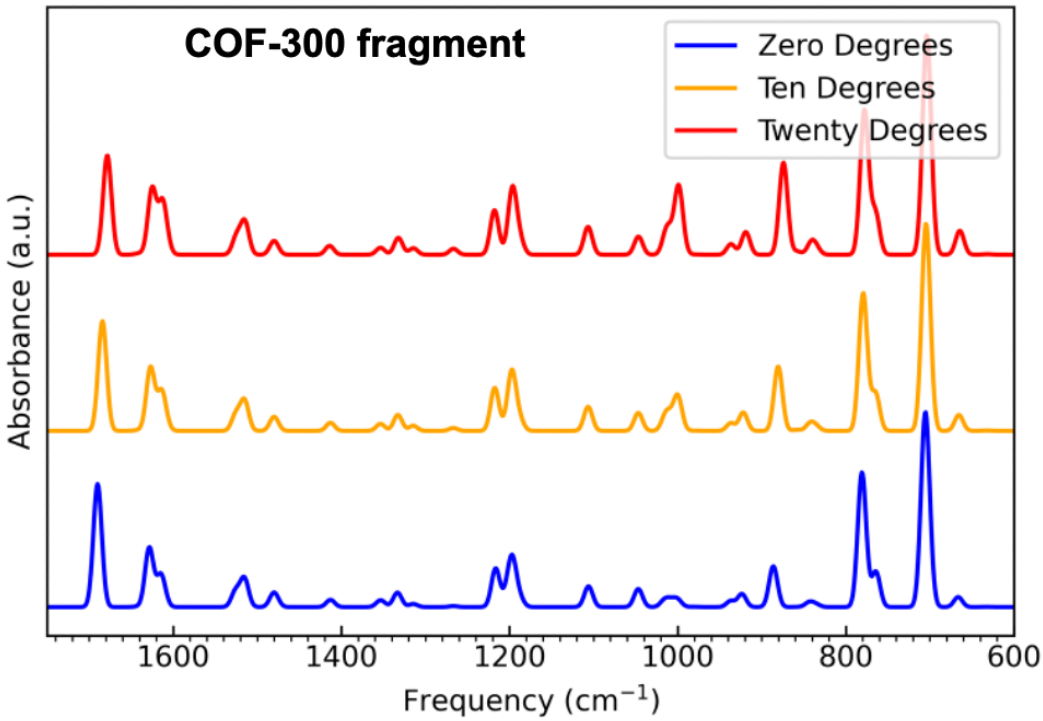

Figure S14. Simulated IR spectra of COF-300 molecular fragment (*N*-benzylideneaniline) showing results of rotation (via the pedal motion) about the imine functionality as a function of varying the C-C=N-C angle. Calculated at B3LYP/6-311G++(d,p), including empirical dispersion (DFT-D3), with the stick spectrum convolved with a Gaussian for comparison with experiment.

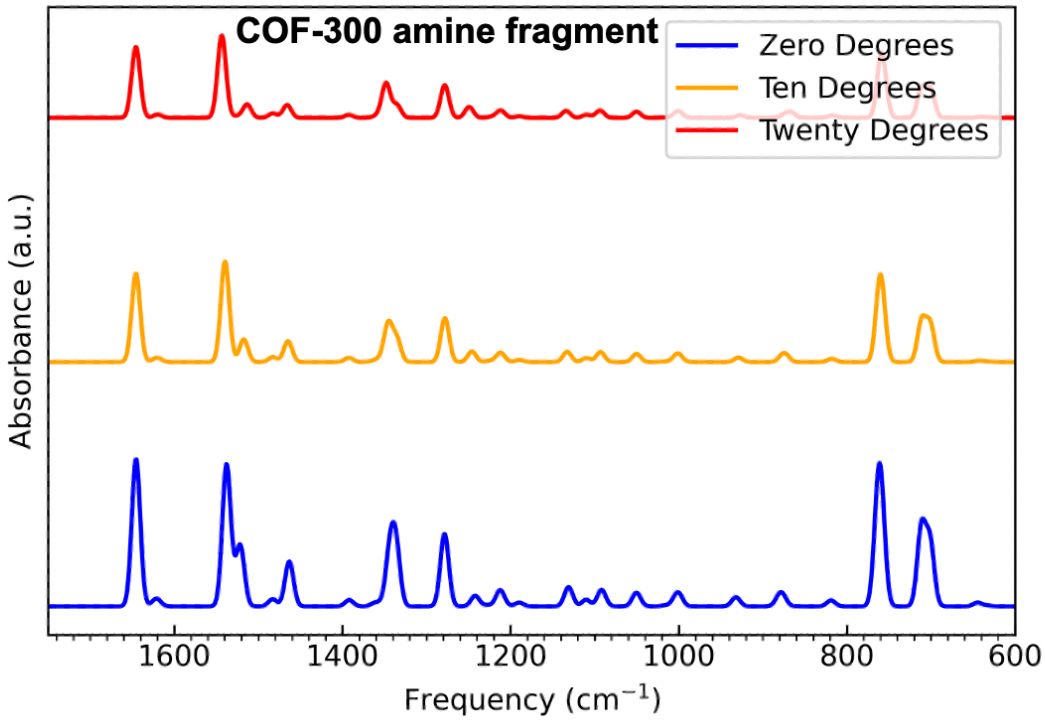

Figure S15. Simulated IR spectra of COF-300-amine molecular fragment (*N*-benzylaniline) showing results of rotation (via the pedal motion) about the amine functionality as a function of varying the C-C-N-C angle. Calculated at B3LYP/6-311G++(d,p), including empirical dispersion (DFT-D3), with the stick spectrum convolved with a Gaussian for comparison with the experiment.

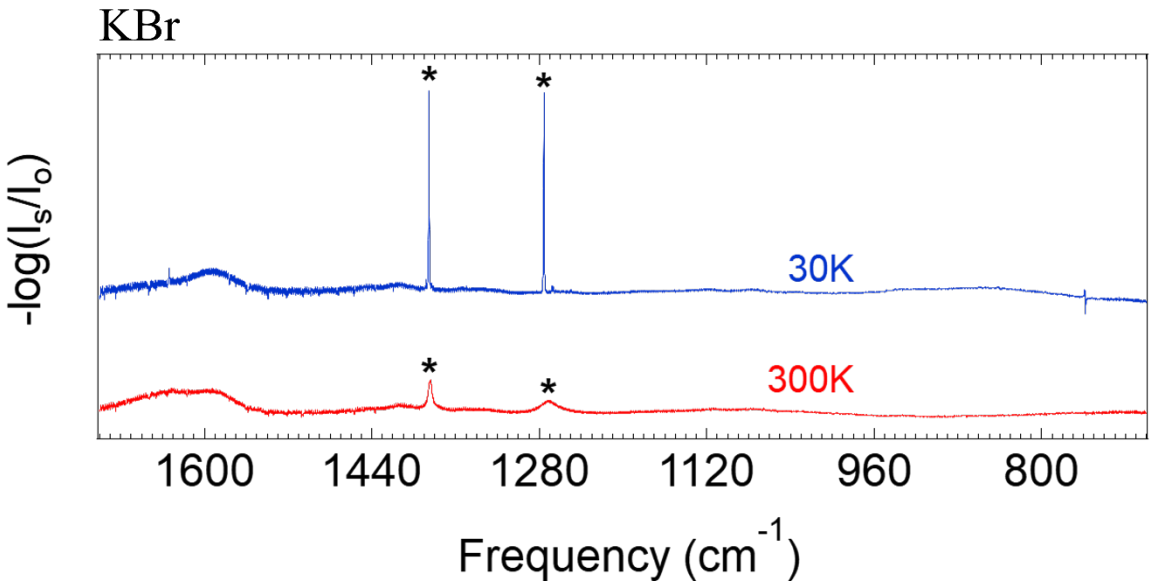

Figure S16. Room-temperature and cryogenic IR spectra of KBr without any added framework materials. Peaks with asterisks, at 1385 and 1275 cm^{-1}, are identified as either water or carbon dioxide impurities based on previous literature.[13]

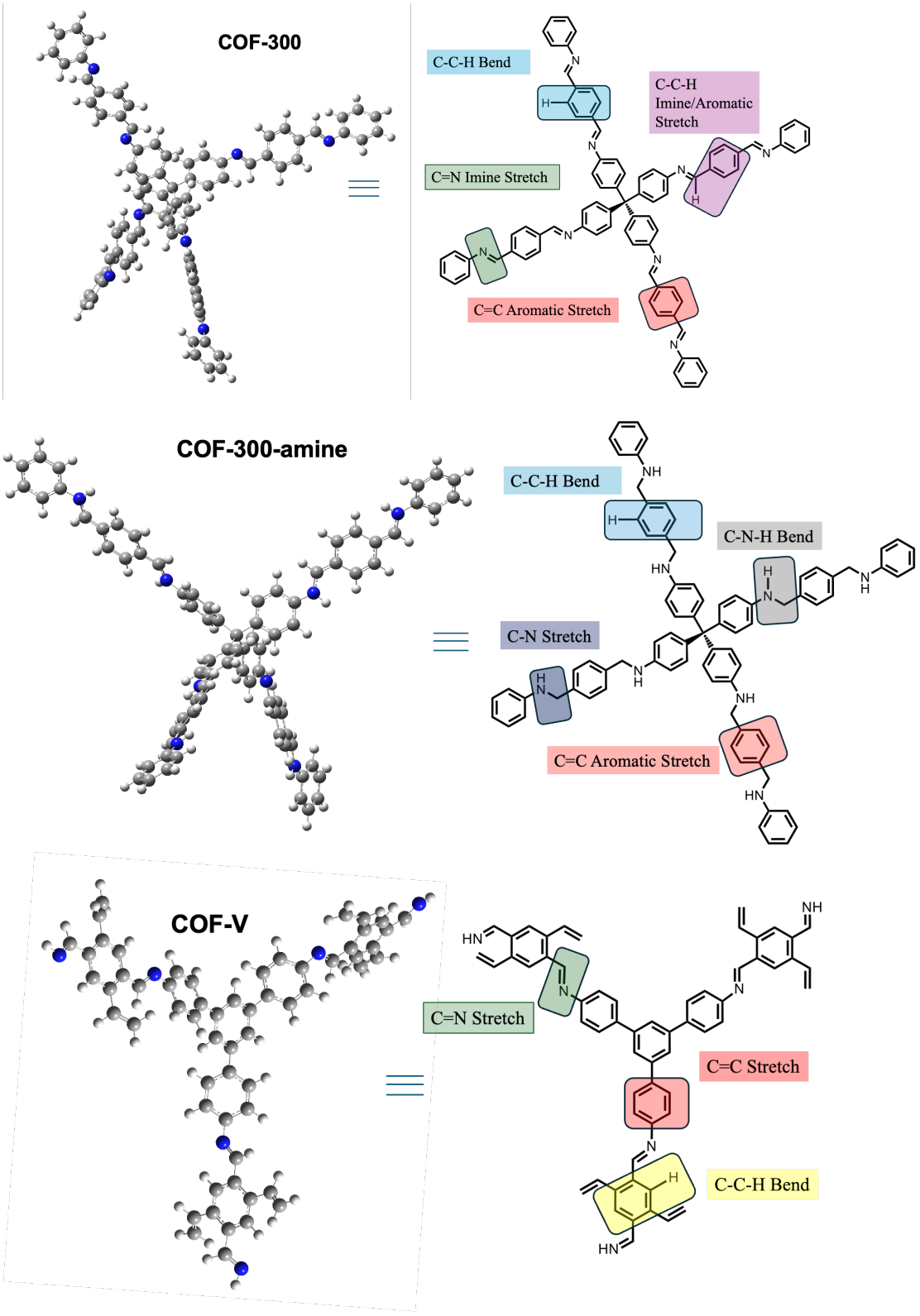

Figure S17. Cluster models of COFs.

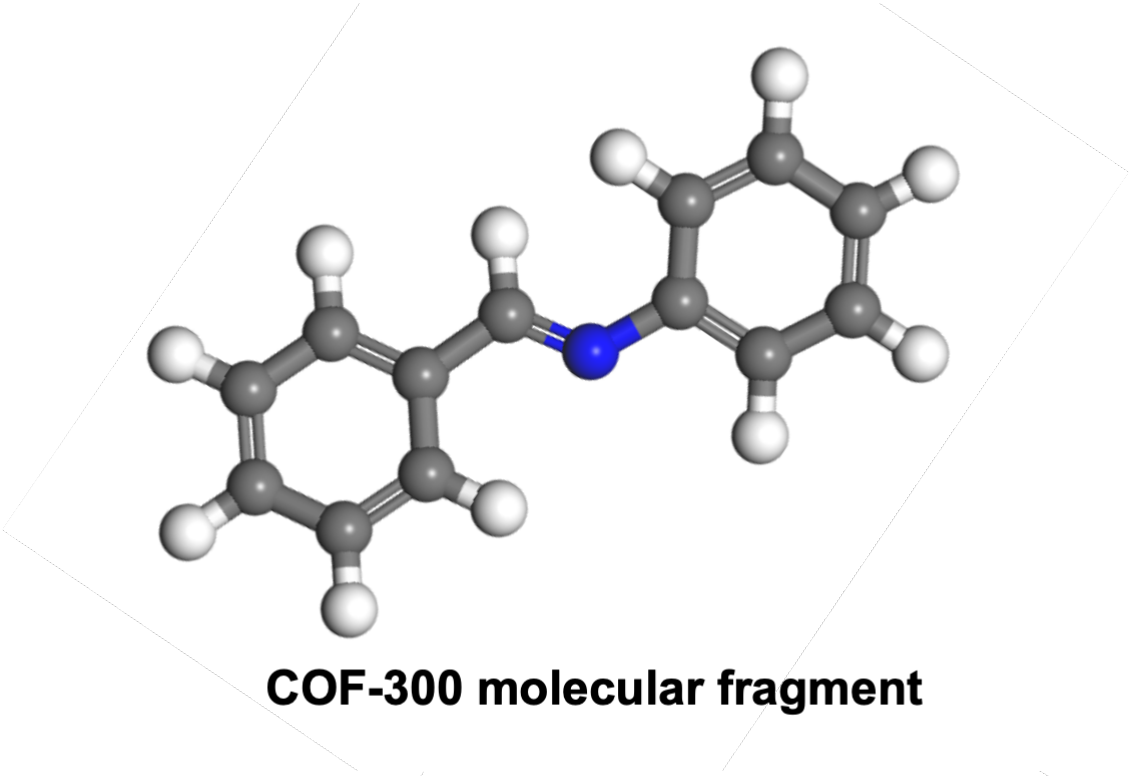

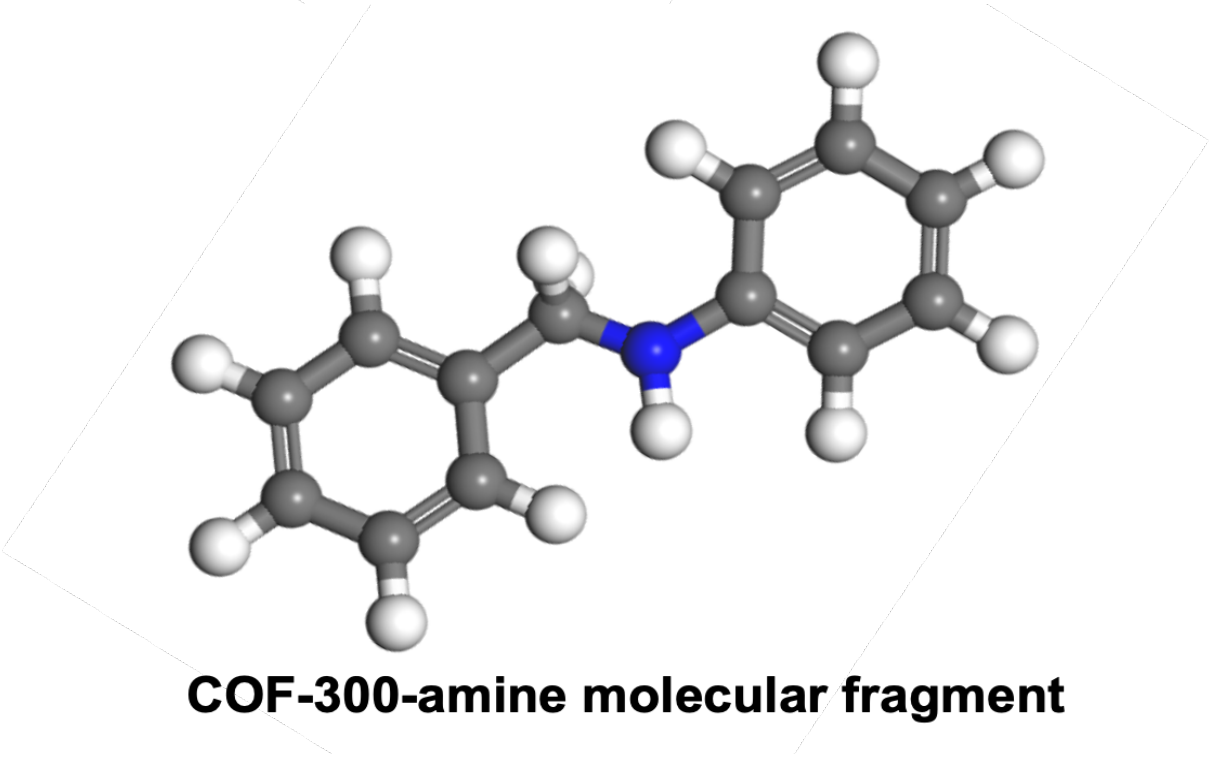

Figure S18. Molecular fragments of COF-300 and COF-300-amine

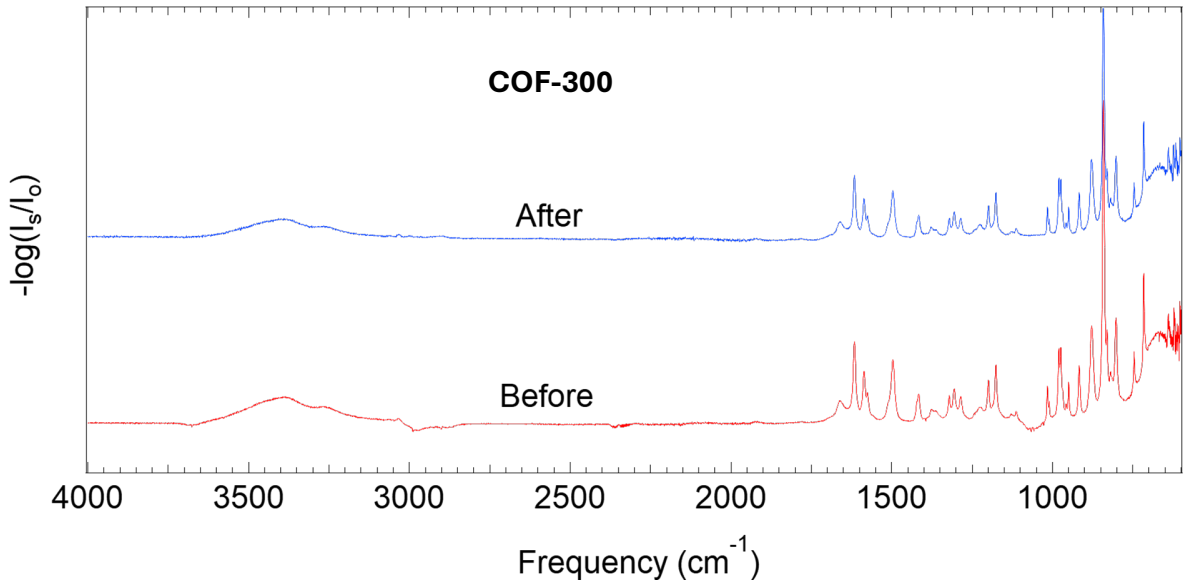

Figure S19. IR spectra for COF-300, before and after sample pressing (12 tons/in^2). Spectra were collected at room temperature in air with unactivated sample, without KBr.

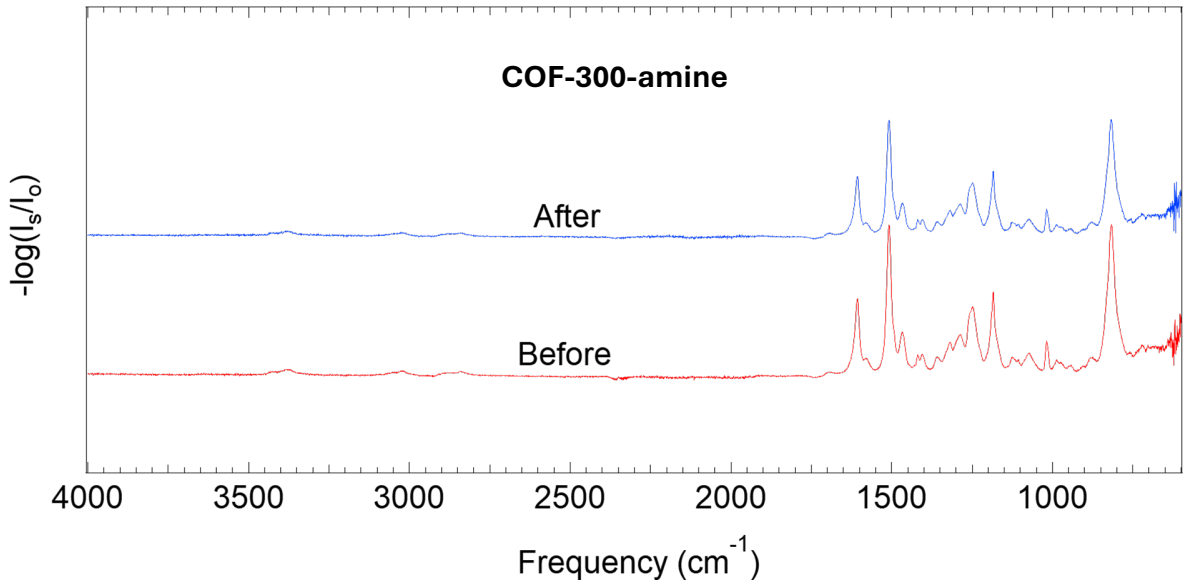

Figure S20. IR spectra of COF-300-amine, before and after sample pressing (12 tons/in^2) . Spectra were collected at room temperature in air with unactivated sample, without KBr.

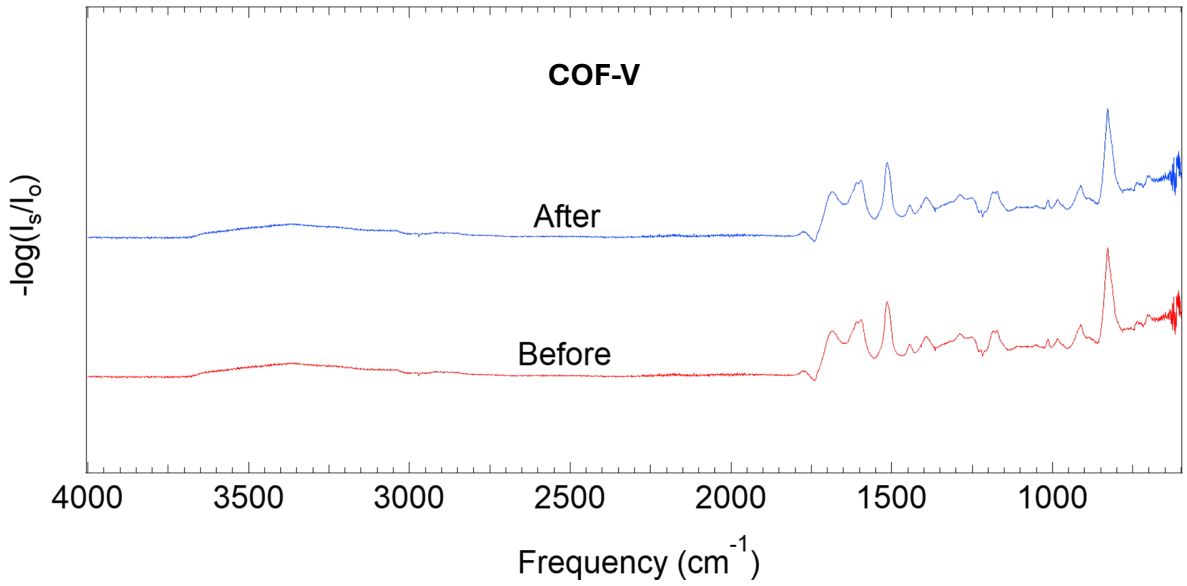

Figure S21. IR spectra of COF-V before and after sample pressing (12 tons/in^2). Spectra were collected at room temperature in air with unactivated sample, without KBr.

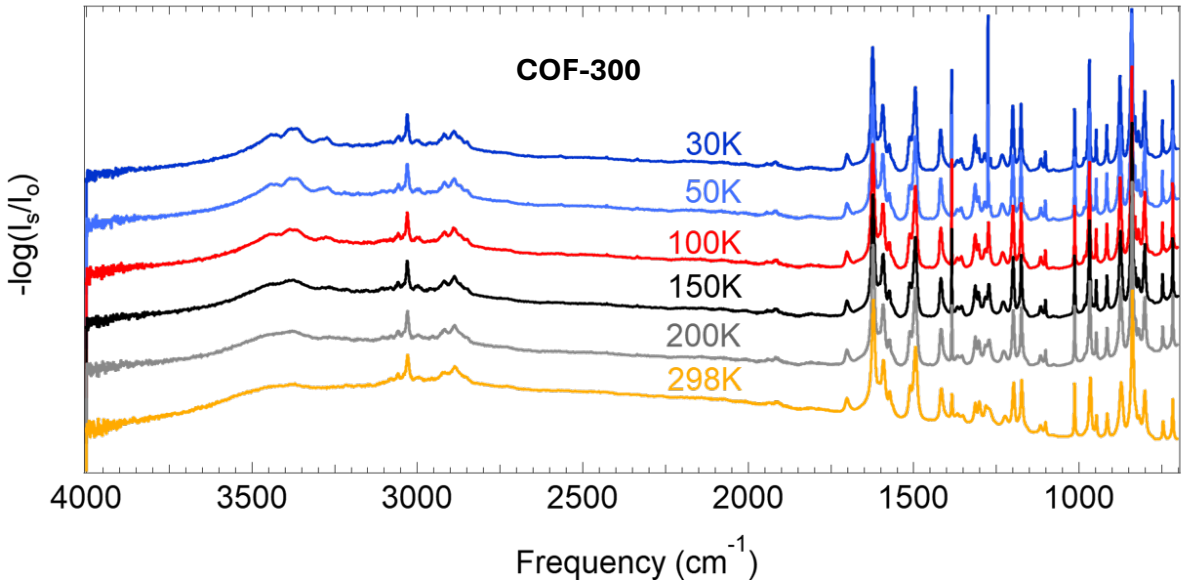

Figure S22. FTIR spectra at varying temperatures for COF-300 showing high wavenumber regions.

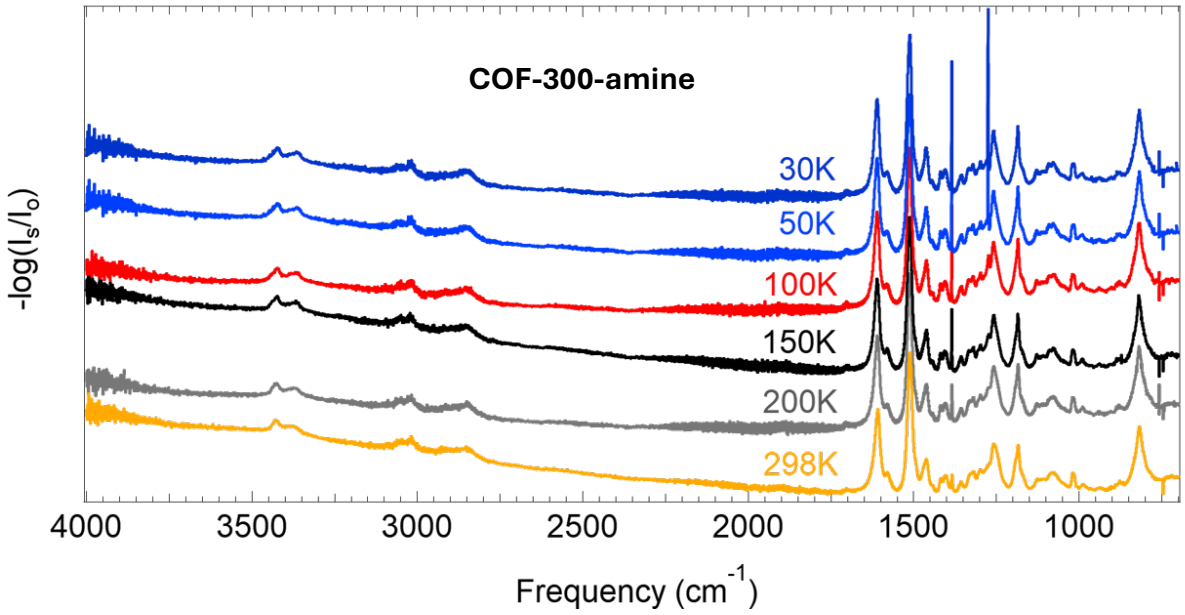

Figure S23. FTIR spectra at varying temperatures for COF-300-amine showing high wavenumber regions.

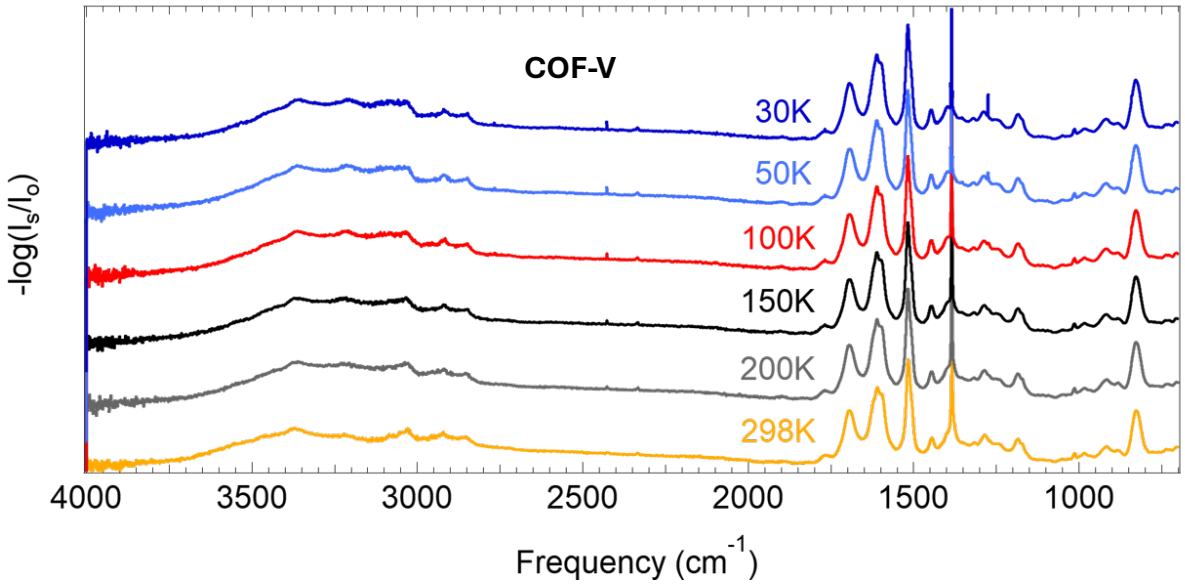

Figure S24. FTIR spectra at varying temperatures for COF-V showing high wavenumber regions.

Supplementary Tables:

Table S1: Vibrational frequencies calculated for the COF-300 molecular fragment at three different C-N=C-C dihedral angles (0°, 10°, and 20°), calculated at B3LYP/6-311G++(d,p), including empirical dispersion (DFT-D3). Also reported is the change in frequency for each mode relative to the global minimum (defined to be 0°), where Δ(X°−0°) is defined as the difference in frequencies of the corresponding vibrational mode in the rotated C-N=C-C dihedral angle X degrees from the same mode at 0°.

angle = 0° Frequency (cm^{-1})	angle = 10° Frequency (cm^{-1})	angle = 20° Frequency (cm^{-1})	Δ(10°− 0°) (cm^{-1})	Δ(20°− 0°) (cm^{-1})
39.6	41.3	41.9	1.7	2.3
57.9	56.3	54.1	−1.6	−3.7
71.6	67.8	65.0	−3.9	−6.6
134.3	148.6	155.2	14.3	20.8
188.5	183.8	181.0	−4.8	−7.5
249.9	255.0	258.0	5.1	8.1
283.5	296.1	301.4	12.6	17.9
344.9	339.5	337.1	−5.4	−7.9
413.8	413.8	413.8	0.0	−0.1
421.3	422.6	423.2	1.3	1.8
463.0	463.2	462.3	0.2	−0.7
523.5	522.1	519.8	−1.4	−3.7
541.3	540.9	539.9	−0.4	−1.4
552.9	550.2	547.5	−2.6	−5.4
630.3	630.1	629.8	−0.3	−0.6
633.5	633.2	632.9	−0.3	−0.6
666.4	665.5	664.4	−0.8	−2.0
702.5	702.3	701.8	−0.1	−0.7
706.0	705.3	704.3	−0.7	−1.7
764.2	764.7	764.8	0.5	0.5
780.8	779.4	777.9	−1.4	−2.9
835.7	835.4	835.0	−0.3	−0.7
843.6	842.4	841.0	−1.2	−2.6
858.1	858.1	858.0	0.0	0.0
886.2	880.4	874.2	−5.8	−12.1
923.6	922.0	919.0	−1.6	−4.6
937.0	936.8	936.6	−0.1	−0.4
979.1	978.2	977.2	−0.9	−2.0
991.9	992.8	993.2	0.8	1.3

995.9	994.7	993.7	−1.3	−2.2
1000.7	1000.0	998.9	−0.7	−1.8
1009.1	1009.3	1009.4	0.2	0.3
1014.6	1014.6	1013.7	0.0	−0.9
1016.0	1014.7	1014.6	−1.3	−1.4
1045.9	1046.1	1046.0	0.1	0.0
1047.1	1046.9	1046.7	−0.2	−0.4
1105.7	1106.1	1106.0	0.3	0.2
1106.2	1106.8	1107.1	0.7	0.9
1187.6	1187.5	1187.3	−0.1	−0.3
1191.2	1191.2	1191.2	0.0	0.0
1196.7	1197.2	1196.5	0.4	−0.2
1202.5	1202.8	1202.8	0.3	0.3
1216.5	1217.5	1217.9	1.1	1.4
1266.8	1266.8	1266.6	0.0	−0.2
1314.5	1314.5	1314.3	0.0	−0.2
1333.3	1332.8	1332.2	−0.5	−1.1
1351.0	1352.0	1352.4	1.0	1.4
1354.3	1354.1	1354.0	−0.1	−0.3
1413.0	1413.0	1414.0	0.1	1.1
1478.0	1477.8	1477.6	−0.2	−0.4
1480.8	1480.6	1480.6	−0.2	−0.2
1515.4	1515.2	1514.8	−0.2	−0.6
1525.9	1525.4	1524.7	−0.5	−1.2
1611.1	1608.8	1606.8	−2.4	−4.3
1615.0	1614.0	1612.7	−1.0	−2.2
1628.5	1627.0	1625.1	−1.5	−3.3
1642.1	1641.4	1640.5	−0.6	−1.5
1690.0	1684.2	1678.4	−5.8	−11.5
2995.6	2984.3	2969.9	−11.3	−25.7
3154.5	3155.0	3155.5	0.5	1.0
3158.2	3158.4	3158.3	0.2	0.1
3163.8	3164.0	3164.3	0.3	0.6
3166.1	3166.2	3166.1	0.1	−0.1
3175.2	3175.4	3175.6	0.2	0.4
3176.8	3178.0	3178.3	1.2	1.5
3184.4	3184.5	3184.5	0.1	0.1
3187.0	3187.0	3187.1	0.1	0.2
3191.3	3191.2	3191.1	−0.2	−0.2
3196.6	3196.2	3196.0	−0.3	−0.5

Table S2: Vibrational frequencies calculated for the COF-300-amine molecular fragment at three different C-N-C-C dihedral angles (0°, 10°, and 20°), calculated at B3LYP/6-311G++(d,p), including empirical dispersion (DFT-D3).Also reported is the change in frequency for each mode relative to the global minimum (defined to be 0°), where Δ(X°−0°) is defined as the difference in frequencies of the corresponding vibrational mode in the rotated C-N-C-C dihedral angle X degrees from the same mode at 0°.

angle = 0° Frequency (cm^{-1})	angle = 10° Frequency (cm^{-1})	angle = 20° Frequency (cm^{-1})	Δ(10°− 0°)	Δ(20°− 0°)
18.0	21.1	21.1	3.1	3.1
38.4	34.6	28.5	−3.8	−9.9
65.6	62.2	54.2	−3.4	−11.4
96.5	102.1	109.0	5.5	12.5
172.2	174.9	176.4	2.7	4.2
228.5	224.8	219.0	−3.8	−9.5
245.9	245.5	248.3	−0.4	2.4
343.6	331.9	320.4	−11.8	−23.2
401.2	385.4	344.1	−15.8	−57.1
413.5	413.9	414.1	0.4	0.6
417.8	417.4	417.4	−0.4	−0.5
453.9	446.7	440.9	−7.1	−13.0
518.6	516.1	513.9	−2.5	−4.7
541.5	537.4	531.1	−4.1	−10.4
550.0	545.9	544.6	−4.1	−5.4
631.4	630.9	630.5	−0.4	−0.9
635.2	635.0	634.7	−0.2	−0.4
644.7	642.9	640.6	−1.7	−4.0
701.1	700.8	700.6	−0.3	−0.5
711.3	711.1	711.3	−0.3	0.0
758.9	758.0	756.8	−0.9	−2.1
763.4	761.4	759.8	−2.1	−3.7
818.7	817.4	815.8	−1.3	−3.0
819.9	819.6	818.8	−0.3	−1.2
857.2	857.6	857.8	0.5	0.6
876.2	872.8	866.3	−3.5	−9.9
880.7	877.4	874.4	−3.3	−6.3
932.0	928.9	926.6	−3.1	−5.4
963.3	963.2	962.9	−0.1	−0.4
980.5	980.2	979.6	−0.3	−0.9

984.5	985.1	985.8	0.6	1.4
999.6	999.1	999.1	−0.5	−0.6
1001.5	1001.8	1002.0	0.3	0.5
1006.9	1006.4	1005.8	−0.4	−1.1
1017.6	1017.4	1017.2	−0.2	−0.5
1048.4	1048.2	1047.9	−0.2	−0.4
1050.4	1050.4	1050.3	−0.1	−0.1
1091.8	1093.0	1093.6	1.2	1.8
1110.1	1109.8	1109.7	−0.4	−0.4
1131.0	1132.7	1133.9	1.7	3.0
1189.6	1189.6	1189.5	0.0	−0.1
1190.5	1190.4	1190.3	−0.2	−0.2
1208.6	1208.3	1208.1	−0.3	−0.5
1212.6	1212.2	1212.0	−0.4	−0.5
1227.5	1224.5	1222.6	−3.0	−4.9
1242.1	1246.0	1249.2	3.9	7.1
1278.5	1278.1	1278.3	−0.4	−0.2
1336.3	1335.4	1335.2	−0.9	−1.1
1343.6	1345.6	1347.9	1.9	4.3
1356.2	1355.4	1354.9	−0.8	−1.3
1362.1	1361.7	1361.5	−0.4	−0.6
1391.9	1392.3	1392.3	0.4	0.4
1463.2	1464.7	1465.8	1.5	2.6
1482.9	1482.8	1482.8	−0.2	−0.1
1521.4	1517.3	1513.3	−4.1	−8.1
1522.9	1523.1	1523.5	0.2	0.6
1528.2	1527.8	1527.4	−0.4	−0.8
1537.8	1539.6	1543.4	1.8	5.6
1620.7	1620.0	1619.4	−0.7	−1.4
1624.5	1624.5	1624.5	0.0	0.1
1645.1	1645.1	1644.8	−0.1	−0.3
1646.1	1646.2	1646.2	0.1	0.1
2966.5	2963.5	2963.8	−3.0	−2.7
3019.2	3023.1	3029.3	4.0	10.2
3147.1	3146.9	3146.4	−0.2	−0.7
3154.9	3154.4	3153.9	−0.5	−1.0
3159.7	3159.7	3159.5	0.0	−0.2
3160.2	3160.4	3160.3	0.2	0.1
3169.1	3169.0	3168.7	−0.1	−0.4
3169.5	3169.8	3169.8	0.3	0.3

3178.0	3178.1	3178.1	0.2	0.1
3186.9	3187.1	3187.0	0.2	0.2
3188.1	3187.9	3187.8	−0.1	−0.2
3194.8	3195.2	3194.7	0.4	−0.1
3596.6	3604.4	3617.0	7.7	20.3

Reference

1. P. Ganesan, X. Yang, J. Loos, T. J. Savenije, R. D. Abellon, H. Zuilhof and Ernst, *Journal of the American Chemical Society*, 2005, **127**, 14530–14531.
2. Christoph Klumpen, M. Breunig, T. Homburg, N. Stock and J. Senker, *Chemistry of Materials*, 2016, **28**, 5461–5470.
3. A. Palma-Cando, E. Preis and U. Scherf, *Macromolecules*, 2016, **49**, 8041–8047.
4. J. Lu and J. Zhang, *J. Mater. Chem. A*, 2014, **2**, 13831–13834.
5. A. N. Zeppuhar, D. S. Rollins, D. L. Huber, E. A. Bazan-Bergamino, F. Chen, H. A. Evans and M. K. Taylor, *ACS Applied Materials & Interfaces*, DOI:https://doi.org/10.1021/acsami.3c12826.
6. F. D. Bellamy and K. Ou, *Tetrahedron Letters*, 1984, **25**, 839–842.
7. H. Liu, J. Chu, Z. Yin, X. Cai, L. Zhuang and H. Deng, *Chem*, 2018, **4**, 1696–1709.
8. K. Yoshida, H. Takahashi and T. Imamoto, *Chemistry*, 2008, **14**, 8246–8261.
9. Alejandro, D. Rodríguez-San-Miguel, K. C. Stylianou, M. Cavallini, D. Gentili, F. Liscio, S. Milita, Otello Maria Roscioni, M. Luisa Ruiz-González, C. Carbonell, D. Maspoch, Rubén Mas-Ballesté, J. L. Segura and F. Zamora, *PubMed*, 2015, **21**, 10666–10670.
10. F. J. Uribe-Romo, J. R. Hunt, H. Furukawa, C. Klöck, M. O'Keeffe and O. M. Yaghi, *Journal of the American Chemical Society*, 2009, **131**, 4570–4571.
11. W. Ma, Q. Zheng, Y. He, G. Li, W. Guo, Z. Lin and L. Zhang, *Journal of the American Chemical Society*, 2019, **141**, 18271–18277.
12. X. Tang, Q. Zhang, D. Chen, L. Deng, Y. He, J. Wang, C. Pan, J. Tang and G. Yu, *Chemical communications*, 2023, **59**, 8731–8734.
13. V. M. Malhotra, S. Jasty and R. Mu, *Applied Spectroscopy*, 1989, **43**, 638–645.